Solubilization of free β-sitosterol in milk sphingomyelin and polar lipid vesicles as carriers: Structural characterization of the membranes and sphingosome morphology

Christelle Lopez, Elisabeth David Briand, Virginie Lollier, Cristelle Mériadec, Thomas Bizien, Javier Pérez, Franck Artzner

Solubilisation of free β-sitosterol in milk sphingomyelin and polar lipid vesicles as carriers: structural characterization of the membranes and sphingosome morphology

Christelle Lopez [a,b,*], Elisabeth David-Briand [a], Virginie Lollier [a,c], Cristelle Mériadec [d], Thomas Bizien [e], Javier Pérez [e], Franck Artzner [d]

[a] INRAE, BIA, F-44316, Nantes, France

[b] INRAE, STLO, F-35000, Rennes, France

[c] INRAE, PROBE Research Infrastructure, BIBS Facility, F-44316, Nantes, France

[d] IPR, UMR 6251, CNRS, University of Rennes 1, F-35042, Rennes, France

[e] Synchrotron Soleil, L'Orme des Merisiers, Saint-Aubin BP48, F-91192, Gif-sur-Yvette, France

*Corresponding author : Christelle LOPEZ

christelle.lopez@inrae.fr

ABSTRACT

High consumption of plant sterols reduce the risk of cardiovascular disease in humans and provide health benefits. Increasing their amount in the diet is necessary to reach the recommended daily dietary intake. However, food supplementation with free plant sterols is challenging because of their low solubility in fats and water. The objectives of this study were to investigate the capacity of milk-sphingomyelin (milk-SM) and milk polar lipid vesicles to solubilise β-sitosterol molecules in bilayer membranes organised as vesicles called sphingosomes. The thermal and structural properties of milk-SM containing bilayers composed of various amounts of β-sitosterol were examined by differential scanning calorimetry (DSC) and temperature-controlled X-ray diffraction (XRD), the molecular interactions were studied using the Langmuir film technique, the morphologies of sphingosomes and β-sitosterol crystals were observed by microscopy. We showed that the milk-SM bilayers devoid of β-sitosterol exhibited a gel to L_α phase transition for T_m = 34.5°C and formed facetted spherical sphingosomes below T_m. The solubilisation of β-sitosterol within milk-SM bilayers induced a liquid-ordered L_o phase above 25 %mol (1.7 %wt) β-sitosterol and a softening of the membranes leading to the formation of elongated sphingosomes. Attractive molecular interactions revealed a condensing effect of β-sitosterol on milk-SM Langmuir monolayers. Above 40 %mol (25.7 %wt) β-sitosterol, partitioning occured with the formation of β-sitosterol microcrystals in the aqueous phase. Similar results were obtained with the solubilisation of β-sitosterol within milk polar lipid vesicles. For the first time, this study highlighted the efficient solubilisation of β-sitosterol within milk-SM based vesicles, which opens new market opportunities for the formulation of functional foods enriched in non-crystalline free plant sterols.

Keywords : plant sterol, phytosterol, functional food, membrane bilayer, milk polar lipid, sphingolipid, encapsulation, liposome

1. Introduction

The consumer's demand for food products and beverages delivering health benefits and preventing diseases has increased over the years. In the next years, a major challenge for the food industry will therefore consist in producing nutritionnally interesting and healthy foods (Battacchi et al., 2020; Román et al., 2017), including functional foods supplemented in health-promoting bioactive compounds that contribute in the dietary primary prevention, for example plant sterols to decrease the risk of cardiovascular diseases in adults. However, the supplementation of bioactive molecules into foods and beverages is often limited by their low solubility in water and fats. Innovation in the design of encapsulation systems able to improve the solubilisation of dietary bioactives, such as plant sterols, into foods requires further research studies.

Plant sterols, also known as phytosterols (including phytostanols), are found naturally in a range of plant-based foods (vegetables, fruits, cereals, nuts, seeds) in concentrations of up to 5%, with the highest concentrations occurring in vegetable oils (Ostlund, 2002; Weihrauch and Gardner, 1978) except refined oils such as palm oil. They are lipophilic essential constituents of the cell membrane of plants. In many plant-based foods, β-sitosterol is the most abundant sterol form in mass, followed by stigmasterol and campesterol (Ostlund, 2002).

The main interest in plant sterols lies in their potential to act as cholesterol-lowering agents and then as natural preventive dietary products towards cardiovascular disease (Moreau et al., 2018; Turini et al., 2022). Plant sterols also possess anti-carcinogenic and anti-inflammatory properties (Chawla et al., 2016; Rocha et al., 2016). The effects of plant sterols depend on the dose and formulation of the food matrix including the physical form (solubilised vs crystallised plant sterols) and on their fate upon digestion (Clifton, 2015; Plat et al., 2012). An intake of 1.5 –3 g/day of plant sterols has been shown to produce a 10–15% reduction in low-density lipoprotein (LDL) cholesterol in humans (Cusack et al., 2013; Kritchevsky and Chen, 2005; Ostlund, 2002; Piironen et al., 2000). Several studies have suggested that the LDL-cholesterol lowering effect of plant sterols reaches a maximum at doses of 2–3 g/day (Katan et al., 2003; Law, 2000; Musa-Veloso et al., 2011; Parraga-Martinez et al., 2015; Plat et al., 2012; Ras et al., 2014). Intakes of 2 g/day plant sterols in the diet have not been linked to adverse effects on health in long-term human studies (Gylling et al., 2014), and plant sterols are therefore considered GRAS (generally recognized as safe). However, controversies exist about the increased dietary exposure to plant sterols and their potential adverse effects. Expanded

research has emerged with the identification of plant sterols together with plant sterol oxidation products (POPs) accumulated in arterial lesions. POPs exhibit pro-atherogenic properties, cytotoxicity oxidative stress, apoptosis, and pro-inflammatory properties and have therefore a negative impact on human health (Alemany et al., 2014; Feng et al., 2020; Scholz et al., 2015).

Health authorities edited lifestyle guidelines to manage hypercholesterolemia and they recommended intakes for plant sterols including 2 g/day in the human diet as an optimal dose (Plat et al., 2012), for example the U.S. National Cholesterol Education Program for lifestyle changes to lower serum cholesterol (Expert Panel on Detection, Evaluation, and Treatment of High Blood Cholesterol, 2001) and others (American Heart Association Nutrition Committee et al., 2006; Grundy et al., 2014; Gylling et al., 2014). In the typical Western diet, natural dietary intake of plant sterols varies from about 150 to 440 mg/day (Berger et al., 2004; Lagarda et al., 2006; Ostlund, 2002; Piironen et al., 2000). Since the worldwide population does not meet the recommended intakes for plant sterols, increasing the amount of plant sterols consumed in a variety of foods, i.e. plant sterols provided by a natural diet including vegetable oils (intrinsic plant sterols) and supplementation in plant sterols (added plant sterols), may be an important way of reducing significantly population LDL-cholesterol levels and preventing coronary heart disease (Berger et al., 2004).

Supplementing foods and beverages with plant sterols is a strategy accepted by scientists, food manufacturers, and consumers. Plant sterols are therefore widely used as functional food ingredients (Jesch and Carr, 2017). However, the successful incorporation of plant sterols in functional foods is really challenging from a technological and food quality standpoint, since plant sterols are poorly soluble in dietary fats and insoluble in water where they adopt a crystalline form. Purified plant sterols, i.e. the form in which they are usually commercially supplied, form highly stable microcrystals with a high melting point (140-170°C ; (Acevedo and Franchetti, 2016)), that are difficult to dissolve in intestinal bile salt solutions and limit their absorption in the gastrointestinal tract (Salo and Wester, 2005). Authors reported that the consumption of 10–20 g/day of crystalline plant sterols had a comparable effect (e.g., a 10% reduction in the LDL-cholesterol level) with 2 g/day of solubilized free plant sterols (Engel and Schubert, 2005; Izadi et al., 2012). Direct dissolution of free plant sterols in fat is not very efficient because their solubility in triglyceride is only about 1 to 2%. Researchers have reported that when free plant sterols are effectively heated above their melting temperature and then recrystallized in fat upon cooling, they become bioavailable and therefore effective in reducing cholesterol absorption (Hayes et al., 2004). Recrystallization of free plant sterols in fat has been

studied (Acevedo and Franchetti, 2016), as well as the solubilisation of free plant sterols in oil-in-water dairy emulsions (Zychowski et al., 2016). An other solution to increase the solubility of plant sterols is a chemical method : the esterification of plant sterols with long-chain fatty acids (e.g., β-sitosteryl oleate versus free β-sitosterol) has been reported to increase their solubility in fat to 10–20% (Mattson et al., 1982; Vanhanen et al., 1993). Up to this time, the addition of chemically modified plant sterol fatty acid esters to processed fat containing foods is prevalent in the food industry. The fat-solubility of plant sterol esters allows delivery of several grams daily in fatty foods such as margarine (Law, 2000). For examples, the margarines Benecol® and Take Control® contain plant sterol esters to increase the amount of plant sterol in the product relative to fat. However, this approach is not favorable to people who are on low fat diet. Furthermore, free plant sterols can lower LDL-cholesterol levels more than their esterified counterparts (Shaghaghi et al., 2014).

Other strategies dedicated to the solubilisation of plant sterols for food applications include physical encapsulation methods. For example, spray-drying microencapsulation, spray-chilling, solid lipid nanoparticles, nanostructured lipid carrier, and emulsification are the most employed to encapsulate phytosterols (Chemin et al., 2008; da Silva et al., 2022; Pavani et al., 2022; Tolve et al., 2020), and their advantages have been recently reported (Pavani et al., 2022). These advanced technologies have a great potential for the solubilisation and protection of plant sterols during processing and storage. However, there is still a need to design and develop new colloidal lipid carriers, such as lipid vesicles, to enhance low fat based encapsulation systems for widespread utilization of free plant sterols in aqueous foods and beverages (Pavani et al., 2022).

Lipid vesicles are attractive encapsulation systems and efficient delivery systems for bioactive compounds and drugs in aqueous systems, which increases their interest for food applications including beverages (McClements, 2015). They provide enhanced stability of encapsulated materials against a range of environmental, enzymatic, and chemical stresses. Lipid vesicles contain an aqueous volume enclosed by a single phospholipid bilayer (unilamellar vesicles or liposomes) or several concentric bilayers (multilamellar vesicles), in which the hydrophobic molecules, such as plant sterols, can be solubilised and entrapped. Most of the lipid vesicles designed for encapsulation are composed of glycerophospholipids (glycerol backbone). For food applications, model systems such as liposomes composed of pure glycerophospholipids (POPC : 1-palmitoyl-2-oleoyl-sn-glycero-3-phosphocholine and DPPC : 1,2-dipalmitoyl-sn-glycero-3-phosphocholine (Jovanović et al., 2018)), and lipid vesicles composed of a natural

mixture of glycerophospholipids such as egg lecithin, soybean phospholipids or polar lipids from the milk fat globule membrane (MFGM) have been mainly investigated for encapsulation (Bezelgues et al., 2009; Farhang et al., 2012; Gülseren and Corredig, 2013; Guner and Oztop, 2017; Singh, 2006; Thompson et al., 2009; Wang et al., 2017; Wechtersbach et al., 2012). For the encapsulation of plant sterols, authors used liposome entrapments using soybean phospholipids (Alexander et al., 2012; Wang et al., 2017) and egg yolk lecithin (Tai et al., 2018).

An other category of lipid vesicles composed of sphingolipids or sphingomyelin (SM ; sphingosine d18:1 base backbone), that are called sphingosomes, has been successfully developed for pharmaceutical and therapeutic applications (Bouzo et al., 2021; Jatal et al., 2022; Nagachinta et al., 2020), and for food applications to encapsulate lutein and tocopherols (Lopez et al., 2022, 2020). Sphingosomes are promising lipid carriers (Yang and Chen, 2022). SM molecules are the most abundant sphingolipids naturally found in biological membranes where they have structural functions. The specific attractive molecular interactions between the NH group of SM and the OH group of cholesterol are preferentially involved in the formation of liquid-ordered lipid domains termed lipid rafts in cell membranes (Simons and Ikonen, 1997; Slotte, 2016), and in the MFGM (Lopez, 2020; Lopez et al., 2010). The specific chemical structure and physical properties of SM molecules are therefore prone to strong hydrogen bonding with OH-containing guest molecules in the bilayer membranes, which is not the case for glycerophospholipids including PC that do not contain the NH group (Slotte, 2016). The natural dietary sources of SM are from animal-derived foods mainly chicken egg yolk and mammal milks with the MFGM that contains 25-45% milk-SM among the polar lipids (Vesper et al., 1999). Milk SM can also be recovered from by-products of the dairy industry containing milk polar lipids such as buttermilks and butterserums (Fontecha et al., 2020; Lopez, 2021; Lopez et al., 2017).

Few studies focused on the membrane properties of lipid vesicles or sphingosomes containing plant sterols and on their morphology by a biophysical multiscale approach (Tai et al., 2018). Differential scanning calorimetry (DSC) and X-ray diffraction (XRD) have been used to examine the thermal properties of lipid membranes exhibiting changes in their physical state as a function and temperature, and to identify the lamellar organisation and packing of the chains, respectively (Chemin et al., 2008; Lopez et al., 2022, 2020). XRD is also useful to detect the presence of crystals in the samples, such as lutein crystals (Lopez et al., 2020) and plant sterol crystals.

In this work, we hypothesised that milk-SM sphingosomes and milk polar lipid vesicles could be efficient hosts to solubilise free plant sterols such as β-sitosterol within their bilayer membranes. Milk-SM and milk polar lipids are natural and fully biocompatible dietary lipids that could be used for the encapsulation of free plant sterols in foods. The objectives of this study were therefore to examine the role of β-sitosterol molecules i) on the thermotropic phase behaviour and structural properties of milk-SM bilayers using DSC and XRD, ii) on their molecular interactions with milk-SM in Langmuir monolayers, and iii) on the morphology of milk-SM/β-sitosterol sphingosomes. In addition and to open perspectives for food applications, this work aimed at examining the solubilisation of β-sitosterol in vesicles composed of a natural extract of milk polar lipids containing milk-SM.

2. Materials and methods

2.1. Materials

Figure 1 shows the chemical structures of β-sitosterol, cholesterol, and milk polar lipids including milk-SM that have been used in this study.

The β-sitosterol powder (purity > 98% ; MW 414.71 g/mol) was purchased from Larodan (Solna, Sweden). Powders of sphingomyelin from bovine milk (milk-SM; purity > 99% ; MW 801.22 g/mol) and cholesterol (purity > 99% ; MW 386.66 g/mol) were purchased from Avanti Polar Lipids (Alabaster, AL, USA). β-sitosterol is a plant sterol (phytosterol) member of the triterpene family composed of a tetracyclic structure including a hydroxyl group, and a side chain in position C-17. The chemical structure of β-sitosterol differs from that of cholesterol in the structure of the C-24 side chain (**Fig 1 A & B**). Milk-SM corresponds to a natural mixture of various SM species ; their molecular structure is *N*-acyl-D-*erythro*-sphingosylphosphorylcholine (**Fig 1 C**). All milk-SM species have phosphorylcholine as the polar head group. The hydrophobic backbone of milk-SM species contains sphingosine (mainly 18:1) and an amide-linked acyl chain. The acyl chains are mainly long and saturated (19% C16:0, 3% C18:0, 1% C20:0, 19% C22:0, 33% C23:0, 20% C24:0) with high melting points, while a minor proportion corresponds to unsaturated chains (3% C24:1*n*-9) (Filippov et al., 2006).

Milk polar lipids from the bovine milk fat globule membrane (MFGM) were used in this study. The main polar lipids were the sphingolipid milk-SM (38.7%), and the glycerophospholipids

phosphatidylcholine (PC; 31.6%), phosphatidylethanolamine (PE; 23.5%) and the anionic phosphatidylinositol (PI; 3.4%) and phosphatidylserine (PS; 2.8%), as previously described (Et-Thakafy et al., 2019). These milk polar lipids contained 65% saturated fatty acids with chain lengths from C10:0 to C24:0. The high amount of milk-SM in the MFGM extract provided the main saturated long fatty acids in the MFGM polar lipid extract, as previously reported (Et-Thakafy et al., 2019). The averaged molecular weight (MW) of the milk polar lipid molecules was calculated to be 757.4 g/mol, as previously determined (Murthy et al., 2015).

For the hydration of the lipids, PIPES buffer (1,4-piperazinediethane sulfonic acid; purity > 99%; Sigma) was prepared with purified water (Milli-Q waters) to reach a concentration of 10 mM. The PIPES buffer contained NaCl 50 mM (Panreac, Germany, purity > 99%) and $CaCl_2$ 5 mM (Panreac, Germany, purity > 98%). The pH of the PIPES buffer was adjusted to pH 6.7 using NaOH 5M.

2.2. Samples preparation

The appropriate amounts of milk-SM, β-sitosterol, cholesterol or milk polar lipid powders were dissolved in chloroform/methanol (4/1 v/v) and mixed from stock solutions in the desired proportions with molar ratios denoted milk-SM/β-sitosterol, milk-SM/cholesterol and milk polar lipids/β-sitosterol. The organic solvents were evaporated under a stream of dry nitrogen. The samples were hydrated in PIPES buffer. The milk-SM sample was prepared to reach the final concentration of 20 %wt milk-SM, for which milk-SM is fully hydrated (Lopez et al., 2018). The milk-SM/β-sitosterol dried mixtures were prepared to reach the final concentration of 20 %wt of milk-SM + β-sitosterol. The samples were expressed as the molar ratio between milk-SM and β-sitosterol. The milk-SM/β-sitosterol samples were as follows : 100/0 %mol (100 %wt milk-SM), 95/5 %mol (97.3/2.7 %wt), 90/10 %mol (94.6/5.4 %wt), 88/12 %mol (93.4/6.6 %wt), 85/15 %mol (91.6/8.4 %wt), 83/17 %mol (90.4/9.6 %wt), 80/20 %mol (88.5/11.5 %wt), 75/25 %mol (85.3/14.7 %wt), 70/30 %mol (81.8/18.2 %wt), 65/35 %mol (78.2/21.8 %wt), 60/40 %mol (74.3/25.7 %wt) and 50/50 %mol (65.9/34.1 %wt). The milk-SM/cholesterol dried mixtures were prepared to reach the final concentration of 20 %wt of milk-SM + cholesterol and the samples were expressed as the molar ratio and weight ratio between milk-SM and cholesterol as previously reported (Lopez et al., 2018). The milk polar lipids sample was prepared to reach the final concentration of 30 %wt. The milk polar lipids/β-sitosterol mixtures contained a similar amount of milk polar lipids and various amounts of β-sitosterol. The samples were expressed as the molar ratio between milk polar lipids and β-

sitosterol as follows : 100/0 %mol (100 %wt milk polar lipids), 96.1/3.9 %mol (97.8/2.2 %wt), 93.9/6.1 %mol (96.6/3.4 %wt), 91.6/8.4 %mol (95.2/4.8 %wt), 89.1/10.9 %mol (93.7/6.3 %wt), 86.4/13.6 %mol (92.1/7.9 %wt), 80.4/19.6 %mol (88.2/11.8 %wt), 69.5/30.5 %mol (80.6/19.4 %wt). The dispersions were heated at 60°C in order to melt the acyl chains of milk-SM and milk polar lipids as previously determined (Murthy et al., 2015), and thoroughly mixed in a vortex stirrer in order to form large multilamellar vesicles. The samples were kept at 20°C during 4h and at 4°C during at least 24h for equilibration before DSC and XRD analysis.

2.3. Differential scanning calorimetry (DSC)

A calorimeter DSC Q1000 (TA Instruments, Newcastle, DE) was used for DSC measurements, as previously reported in (Lopez et al., 2020). About 10 – 20 mg of β-sitosterol powder or of the milk-SM/β-sitosterol, or milk polar lipids/β-sitosterol samples were loaded into aluminum pans (TA Instruments). The DSC pans were hermetically sealed. The reference was an empty and hermetically sealed aluminum pan. Indium (ΔH = 28.41J/g; Melting point = 156.66°C) was used to calibrate the calorimeter.

The thermotropic behavior of β-sitosterol powder was studied as follows : (i) on heating from 20°C to 200°C at dT/dt = 10°C/min (first heating), (ii) on cooling from 200°C to 20°C at dT/dt = 10°C/min, and then (iii) on heating from 20°C to 200°C at dT/dt = 10°C/min (second heating). The protocol used to examine the thermotropic phase behavior of milk-SM bilayers and milk-SM/ β-sitosterol binary mixtures was as follows : (i) each sample was cooled down to 0°C at dT/dt = 2°C/min, (ii) a first heating scan was run at a rate of dT/dt = 2°C/min from 0°C to 80°C, (iii) a cooling scan was recorded at dT/dt = 2°C/min from 80 to 0°C, and then (iv) a second heating scan was run at a rate of dT/dt = 2°C/min from 0°C to 80°C. To study the thermotropic phase behavior of milk polar lipids/β-sitosterol mixtures, (i) each sample was cooled down to -7°C at 1°C/min in order to crystallize the acyl chains and avoid ice formation in the samples, (ii) a first heating scan was run at a rate of dT/dt = 2°C/min from -7°C to 80°C, (iii) a cooling scan was recorded at dT/dt = 2°C/min from 80 to -7°C, and then (iv) a second heating scan was run at a rate of dT/dt = 2°C/min from -7°C to 80°C. The DSC experiments were performed at least in triplicate for each sample, by preparing and analysing at least three independant pans.

Data analysis was performed using TA Universal Analysis program. The melting transition temperature (T_m) of milk-SM and milk polar lipids bilayers was taken at the peak maximum recorded on heating : the crystallisation transition temperature (T_c) of milk-SM bilayers was

taken at the peak minimum recorded on cooling. Enthalpy changes of the transitions (ΔH_m) were obtained from the area under the peak.

2.4. X-ray diffraction (XRD)

2.4.1. Temperature-controlled XRD

The home-made Guinier beamline at IPR (Rennes, France) was used for X-ray scattering experiments, as already described (Lopez et al., 2020; Lopez et al., 2022). The beamline was equiped with a two-dimensional Pilatus detector with sample to detector distance of 232 mm. Series of concentric rings were recorded in the diffraction patterns as a function of the radial scattering vector $q = 4\pi\sin(\theta)/\lambda$, ($2\theta$: scattering angle ; wavelength of the incident beam λ = 1.541 Å). Silver behenate was used to calibrate the channel to scattering vector q of the detector. Small volumes of samples (around 20 µL) containing milk-SM/β-sitosterol vesicles or milk polar lipids/β-sitosterol vesicles were loaded in thin quartz capillaries of 1.5 mm diameter (GLAS W. Muller, Berlin, Germany) and inserted in the set-up at a controlled temperature, i.e. T = 10-12°C < T_m and T = 60°C > T_m. Each XRD pattern has been recorded for 900 sec. XRD patterns were recorded in the range 0.013 $Å^{-1}$ to 1.742 $Å^{-1}$. This scattering vector q range covered both the small and wide-angles regions of interest to characterize the lamellar structures of milk-SM/β-sitosterol and milk polar lipids / β-sitosterol vesicles and to identify the packing of the acyl chains, respectively. The set-up was also adapted to characterise β-sitosterol crystals in the milk-SM/β-sitosterol samples. PeakFit software (Jandel Scientific, Germany) was used to determine the positions of the Bragg reflections.

2.4.2. Synchrotron-radiation XRD as a function of temperature (XRDT)

The high brilliance of the SWING beamline at the Soleil synchrotron facility was combined with a THMS600 Linkam oven (Linkam Scientific Instruments Ltd, Waterfield, UK) to perform synchrotron-radiation XRD measurements as a function of temperature (XRDT). A EIGERX 4M detector was set at 0.528 m from the sample and the monochromator was set at 15 KeV (David and Pérez, 2009). Thin quartz capillaries of 1.5 mm diameter (GLAS W. Muller, Berlin, Germany) were used to load the samples of β-sitosterol powder, milk-SM and milk-SM/β-sitosterol vesicles. The capillaries were inserted into the THMS600 Linkam oven allowing temperature scan between -194 to 600 °C. For the β-sitosterol powder, the XRDT experiments were conducted on heating from 20°C to 200°C at dT/dt = 10°C/min (940 patterns ; 0.4 sec exposure time and 0.8 sec gap time). For milk-SM and milk-SM/ β-sitosterol (90/10 %mol ;

75/25 %mol) sphingosomes, XRDT experiments were conducted on heating from 10°C to 60°C at dT/dt = 2°C/min (200 patterns ; 2 sec exposure time and 4 sec gap time). Diffraction patterns were recorded for reciprocal spacing q varying between 0.024 and 2.8 $Å^{-1}$, that is, repetitive distances d = 2 π/q ranging from 262 to 2.2 Å. This scattering vector q range allowed the characterization of powdered β-sitosterol crystals, and also covered both the small and wide-angles regions of interest to characterize the lamellar structures of milk-SM molecules and to identify the packing of the acyl chains, respectively. 1D XRD curves were obtained by circular averaging of the 2D images using the Foxtrot software. R software (R Foundation for Statistical Computing, Vienna, Austria) was used to display the three-dimensional plots of XRD patterns as a function of temperature. The positions of the Bragg reflections were determined with PeakFit software (Jandel Scientific, Germany).

2.5. Langmuir film balance experiments

A two-symmetrical barrier Langmuir trough (microtrough XL-LB, Kibron Inc., Helsinki, Finland) was used to perform Langmuir film balance experiments, as previously described (Lopez et al., 2022). The system was equiped with a metallic probe sensor alloy and a hydrophilic oxide. The Langmuir though had a total area of 405 mm × 59 mm and was placed on an anti-vibration table for the experiments. In this study, we recorded surface pressure – area (π – A) isotherms of the different lipid samples, i.e., milk-SM, β-sitosterol, and milk-SM/β-sitosterol mixtures with various molar proportions.

The investigated components were dissolved in chloroform/methanol (4/1 v/v ; analytical grade, Carlo Erba reagents, Val de Reuil, France) to prepare solutions of milk-SM and β-sitosterol with concentrations of 1 mg/ml. The respective stock solutions were mixed to reach the required molar ratio $X_{\beta\text{-sitosterol}}/(1\text{-}X)_{\text{milk-SM}}$. Lipid samples were deposited onto the PIPES buffer sub-phase with a Hamilton micro syringe (precision 0.5 µl). After being spread, the monolayers were left to equilibrate for 10 min. Compression was initiated with a barrier speed of 40 mm^2/min. The experiments were stopped at surface pressure π about 40 $mN.m^{-1}$. Surface pressure π was measured with the accuracy ± 0.1 mN/m. The measurements were performed on PIPES buffer at 20°C. The measurements were performed at least in duplicate for each sample.

The results were reported as surface pressure (π; expressed in mM/m) – area (A; expressed in $Å^2$ per molecule) isotherms. The molecular weights were calculated according to the respective molar proportions of the components in the mixtures for milk-SM and β-sitosterol mixtures.

The magnitude of area condensation due to β-sitosterol addition in the milk-SM/β-sitosterol monolayers was determined as proposed (Gaines, 1966). The theoretical mean area per molecule for milk-SM/β-sitosterol was calculated at two different surface pressures using the following equation: $A = (A_{\beta\text{-sitosterol}} \times X_{\beta\text{-sitosterol}}) + [A_{\text{milk-SM}} \times (1 - X_{\beta\text{-sitosterol}})]$; Wherein $A_{\beta\text{-sitosterol}}$ and $A_{\text{milk-SM}}$ are the molecular areas of the respective components β-sitosterol and milk-SM; and $X_{\beta\text{-sitosterol}}$ and $X_{\text{milk-SM}} = 1 - X_{\beta\text{-sitosterol}}$ are the mole fractions of β-sitosterol and milk-SM respectively. If the two components are immiscible (or ideally miscible) within a mixed monolayer, the area occupied by the mixed film will obey the additive rule and correspond to the sum of the areas of the separated components. A specific interaction between the components will lead to a deviation from the additivity rule. In this case, if the experimental molecular areas of milk-SM/β-sitosterol monolayer are smaller than the theoretical values, this means that a condensing effect of β-sitosterol occurs because of attractive forces with milk-SM.

2.6. Microscopic observations : CLSM combined with DIC

Inverted microscopes NIKON (Eclipse-TE2000-C1si and A1R; NIKON, Champigny sur Marne, France) were used to observe β-sitosterol crystals as well as milk-SM/β-sitosterol and milk-SM/cholesterol sphingosomes, milk polar lipids and milk polar lipids/β-sitosterol vesicles. These microscopes allowed confocal laser scanning microscopy (CLSM) and optical microscopy using differential interferential contrast (DIC). The microstructural analyses were performed at room temperature (e.g. 19 ± 1 °C) using x60 (NA 1.4) or x100 (NA 1.4) oil immersion objectives. The lipid-soluble Nile Red fluorescent dye (9-diethylamino-5H-benzoalpha-phenoxazine-5-one; Sigma–Aldrich, St Louis, USA ; 100 µg/mL in propanediol) was used to stain the bilayers of milk-SM sphingosomes and milk polar lipids vesicles, as previously described (Lopez et al., 2020; Lopez et al., 2022). After the labelling step, the samples were kept at room temperature for at least 15 min. Then, 3 µl of the samples stained with the fluorescent dye were deposited onto the glass and observed on the microscope. The samples were observed with excitation wavelengths of 543 nm (He–Ne laser ; Eclipse-TE2000-C1si microscope) or 561 nm (Sapphire Coherent 561 laser ; A1R microscope). DIC was used to visualize both the lipid vesicles and the β-sitosterol crystals. DIC images were sometimes superimposed to the emission fluorescence recorded in the CLSM images. The two-dimensional images had a resolution of 512 x 512 pixels and the pixel scale values were converted into micrometers using a scaling factor.

3. Results and discussion

3.1. Powdered β-sitosterol crystals

Microscopic observations of the commercial high-purity powder used for the experiments showed that the anhydrous β-sitosterol molecules were organised as microcrystals with a shape of platelets **(Fig 2-A)**. This was in accordance with the platy-like anhydrous β-sitosterol crystals observed by others (Christiansen et al., 2002).

The physical state of the powdered β-sitosterol crystals and their melting behaviour have been examined by synchrotron radiation XRD as a function of temperature and DSC.

The XRD pattern of anhydrous β-sitosterol recorded at 20°C included several reflections corresponding to Bragg distances as indicated **Figure 2-B**. The Bragg distance recorded at small angles at d = 36.3 Å corresponded to the length of the dimeric structure, i.e., 2 molecules of β-sitosterol with hydrogen bonding between the OH-groups as described by (Rossi et al., 2011). These XRD data provided additional information compared to XRD studies performed by synchrotron radiation XRD at small angles (Zychowski et al., 2016) and on lab beamlines at wide angles only, and were in agreement with previous works (Acevedo and Franchetti, 2016; Christiansen et al., 2002; Yang et al., 2018).

The DSC curve recorded on heating of the powdered β-sitosterol crystals exhibited a single sharp endotherm between about 135 and 140 °C (**Fig 2-C**). This endotherm corresponds to the melting of the β-sitosterol crystals. The melting temperature was T_m = 138.2 ± 0.5 °C. The enthalpy of melting was ΔH_m = 41.7 ± 2.1 J/g. These results were in agreement with Acevedo and Franchetti (2016) who found T_m = 137.8 ± 0.8 °C and ΔH_m = 43.3 ± 4.3 J/g. On cooling, the crystallisation temperature of β-sitosterol was T_c = 121.2 ± 0.2 °C. The thermogram recorded during the second heating of β-sitosterol crystals was similar to the thermogram recorded on first heating of the powder, revealing the reversibility of the crystallization and melting properties of the anhydrous β-sitosterol crystals (**Fig 2-C**).

The synchrotron radiation XRD patterns recorded as a function of temperature on heating of β-sitosterol crystals from 20 to 200 °C are presented **Figure 2-D**. The diffraction peaks were the signature of the crystalline state of anhydrous β-sitosterol molecules in the powder. For temperatures above 138 °C, the amorphous state of β-sitosterol molecules was indicated by the

absence of diffraction peaks. The temperature of melting determined by XRDT for anhydrous β-sitosterol crystals, i.e. T_m = 138 °C, was in accordance with DSC results (**Fig 2-C**).

These XRD and DSC measurements showed that β-sitosterol molecules are in a crystalline state below 138 °C. This means that β-sitosterol molecules are in a solid state and organised as microcrystals in a wide range of temperatures, i.e. during technological processing in the food industry, upon storage of foods, and at human body temperature during digestion. This solid state is responsible for the low solubilisation of plant sterols by intestinal bile salts, their low bioaccessibility in the intestinal micelles and their low absorption in the human gastrointestinal tract (Salo and Wester, 2005).

3.2. Milk-SM/β-sitosterol membranes and sphingosomes

3.2.1. Thermotropic phase behaviour of milk-SM/β-sitosterol membranes

The DSC thermograms recorded on heating of the milk-SM/β-sitosterol sphingosomes are presented **Figure 3A**. Changes in the melting temperature T_m and in the enthalpy of melting ΔH_m of milk-SM determined from the DSC thermograms are presented **Figure 3B and C** as a function of the molar percentages of β-sitosterol in the samples.

The thermogram recorded for milk-SM bilayers organised in the form of sphingosomes showed a multicomponent endotherm. This endotherm was composed by a sharp peak with T_m = 34.5 ± 0.3°C, and broad endotherms on both sides. The enthalpy of melting was ΔH_m = 8.9 ± 0.3 kcal/mol. This endothermic event was interpreted as the gel (L_β) - liquid crystalline (L_α) phase transition of milk-SM bilayers, as previously reported (Cheng et al., 2017; Filippov et al., 2006; Lopez et al., 2022, 2018; Murthy et al., 2015; Shaw et al., 2012).

With the increase in the molar proportions of β-sitosterol in the milk-SM/β-sitosterol samples, changes in the endotherms were recorded on heating (**Fig. 3-A**). These changes demonstrated the incorporation of β-sitosterol molecules in the milk-SM bilayers. The incorporation of the guest β-sitosterol molecules in the bilayers composed of the host milk-SM molecules induced i) a decrease in the overall melting enthalpy ΔH_m (**Fig. 3-B**), ii) a decrease in the sharp component of the endotherm that is considered as the main endothermic transition until its disappearance above 20 %mol β-sitosterol, iii) the persistance of the broad component of the endotherm, and iv) a decrease in the melting temperature T_m compared to milk-SM bilayers

alone (**Fig 3-C**). The melting temperature T_m of the sharp component of the DSC endotherm, that is associated to the gel - L_α phase transition, decreased linearly with increases in β-sitosterol amount in the samples. The overall phase transition enthalpy ΔH_m decreased linearly with increasing β-sitosterol concentration. The decreases in T_m and ΔH_m recorded for milk-SM bilayers with increases in the amount of β-sitosterol were similar to results previously obtained for milk-SM/cholesterol bilayers (Lopez et al., 2018) and egg-SM/cholesterol bilayers (Chemin et al., 2008), and milk-SM/α-tocopherol bilayers (Lopez et al., 2022). The enthalpy values determined from the DSC melting events can be associated with the degree of ordering of the milk-SM molecules in the sphingosome bilayers. The decreases in the overall melting enthalpy ΔH_m and in the melting temperature T_m of mixed milk-SM/β-sitosterol bilayers were therefore interpreted as a disorganisation of milk-SM molecules in the gel phase. This disorganisation may be due to a decrease in the hydrophobic interactions between the host milk-SM molecules when the β-sitosterol molecules incorporated the bilayers and then to a decrease in the cooperativity of the milk-SM acyl chains during phase transition, as previously described for SM/cholesterol bilayers (Chemin et al., 2008; Lopez et al., 2018) and milk-SM/α-tocopherol bilayers (Lopez et al., 2022). For β-sitosterol amounts above 30 %mol in the samples, the DSC thermograms did not show any endotherm. This means that the endothermic gel to L_α phase transition did not exist above 30 %mol β-sitosterol in the milk-SM bilayers. A similar thermotropic phase behavior of milk-SM bilayers was reported in presence of cholesterol where the molar proportion of 40 %mol cholesterol corresponded to the completion of the liquid-ordered L_o phase (Lopez et al., 2018).

For all the concentrations in β-sitosterol investigated, the DSC thermograms recorded on heating of milk-SM bilayers were reversible upon cooling and immediate reheating, as reported **Fig 3-D**. These results indicated that the gel - L_α phase transition of milk-SM bilayers did not induce a discharge of β-sitosterol molecules outside the sphingosomes together with structural reorganisations in the membranes as a function of temperature and upon phase transition. This reversibility was also observed for milk-SM bilayers containing cholesterol (Lopez et al., 2018) and egg-SM bilayers loaded with lutein (Lopez et al., 2020).

Our DSC results on the role played by β-sitosterol molecules on milk-SM bilayers were in line with the reduction of the enthalpy and the decrease in the cooperativity of the main endothermic transition measured by DSC with increasing β-sitosterol concentration in pure C16:0-SM and DPPC bilayers (Halling and Slotte, 2004; McKersie and Thompson, 1979).

3.2.2 Structural properties of milk-SM/β-sitosterol bilayers

The structural properties of milk sphingosome membranes alone or in presence of various molar amounts of β-sitosterol were characterised i) by XRD below and above the melting temperature T_m of milk-SM (**Fig 4**) as previously determined by DSC (**Fig 3**), and ii) using high flux synchrotron radiation XRD as a function of temperature for selected samples (**Fig 5**).

Figure 4 shows the XRD patterns that have been recorded at 12 °C (below T_m of milk-SM) and 60 °C (above T_m of milk-SM) for milk-SM/β-sitosterol samples simultaneously at small and wide angles. Milk-SM molecules were organised as lamellar structures (3 reflections noted 01, 02, 03) whatever the temperature and whatever the amount of β-sitosterol in the samples, with a higher thickness of the bilayers at 12 °C compared to 60 °C (**Fig 4 A**). The XRD patterns recorded at wide angles permitted the identification of different packings of the milk-SM acyl chains corresponding to gel phase, L_α phase or L_o phase (**Fig 4 B**).

The 3D representation of the synchrotron radiation XRDT patterns recorded on heating of milk-SM sphingosomes simultaneously at both small and wide angles showed a complex thermotropic phase behaviour (**Fig 5-A**). At 10 °C (below T_m), the reflections recorded at q = 0.08536 $Å^{-1}$ (noted 01), 0.17036 $Å^{-1}$ (noted 02), and 0.25615 $Å^{-1}$ (noted 03) corresponded to a lamellar organisation with a thickness d = 73.6 Å, associated with a single sharp reflection with a Bragg reflection of 4.2 Å attributed to a hexagonal packing (gel phase). At 60°C (above T_m), the main two reflections evolved to q = 0.09279 $Å^{-1}$ (noted 01), and 0.18392 $Å^{-1}$ (noted 02) which corresponded to a thickness of d = 67.7 Å. At wide angles, the broad signal centered at 4.6 Å was interpreted as milk-SM bilayers in the L_α phase. The decrease in the thickness of the lamellar organisation (Δd = -5.9 Å) as a function of the increase in temperature was due to the acyl chain melting and was associated with an increase in the middle height peak with (MHPW) from 0.006515 $Å^{-1}$ (10°C) to 0.014302 $Å^{-1}$ (60°C), indicating a higher disorganisation of the milk-SM chains in the fluid L_α state. The results obtained in the present study for milk-SM bilayers were in agreement with previous reports (Lopez et al., 2022, 2018): milk-SM bilayers exhibited a gel to L_α phase transition with structural reorganizations successively occurring on heating that were attributed to gel phase polymorphism induced by interdigitation of the acyl chains (**Fig 5-A**). In a previous study, we interpreted the complex thermotropic phase behaviour of fully hydrated milk-SM bilayers on heating as follows : i) melting of C16:0-SM, ii) conversion of long and saturated SM species from fully interdigitated (gel-$L_{\beta I}$; 75 Å at 20°C)

to mixed interdigitated (gel-$L_{\beta 2}$; 85 Å at 33°C) lamellar structures and then iii) transition to the fluid L_α phase (Lopez et al., 2018).

In the presence of 10 %mol β-sitosterol in the samples (**Fig 5 B**), the lamellar organisation evolved from 76.1 Å (10°C) with a single peak at wide angles recorded at 1.49 $Å^{-1}$ (d = 4.2 Å) corresponding to an hexagonal packing of the acyl chains, to 72.4 Å with a scattering signal centered at 4.5 Å (60°C) characteristic of the L_α phase. This means that at least part of the milk-SM/β-sitosterol (90/10 %mol) bilayers exhibited a gel to L_α phase transition on heating.

The milk-SM/β-sitosterol samples containing up to 20 %mol β-sitosterol showed a lamellar organisation with a similar shift between 12°C and 60°C due to melting of the milk-SM acyl chains (**Fig 4**). A concentration-dependent effect of β-sitosterol on the milk-SM bilayer structural organisation was observed by wide angle XRD at 12 °C with a progressive decrease in intensity of the Bragg reflection recorded at 4.2 Å (hexagonal packing ; gel phase) that became broader due to changes in the Lamé coefficient as previously discussed for alcohols (Berge et al., 1994). We interpreted this broadening of the wide-angle diffraction peak as an increase in entropy of the acyl chains within the bilayers.

An amount of 25 %mol β-sitosterol in the samples affected the structural properties of the milk sphingosome bilayers (**Fig 4 and 5**). The XRD patterns recorded at small angles on heating of the sample revealed sharp diffraction lines that weakly evolved in position as a function of the increase in temperature, from 76.7 Å (10 °C) to 73.5 Å (60 °C), i.e. Δd = -3.2 Å (**Fig 5 C**). The XRD patterns recorded at wide angles showed a broad and diffuse reflection centered at about 4.5 Å (10-12 °C) and 4.6 Å (60 °C) and the absence of diffraction lines. These structural changes indicated that for 25 %mol β-sitosterol in the samples, the gel to L_α phase transition was eliminated in agreement with DSC experiments (**Fig 3-A**). We concluded that the addition of 25 %mol β-sitosterol in the samples induced the formation of a L_o phase and abolished the gel to L_α phase transition. The L_o phase is in many biophysical respects an intermediate between the gel and L_α phases in the bilayer, with a relatively high degree of translational motion in the plane of the bilayer similar to those in the fluid bilayer although the phospholipid acyl chains are extended and relatively tightly packed, the acyl chain order and phospholipid area compressibility values are more as in the gel-state phospholipids (McMullen et al., 2004). In the range form 0 to 20 %mol β-sitosterol, some but not all of the milk-SM molecules underwent a gel to L_α phase transition (β-sitosterol poor bilayers with properties similar to those of the pure milk-SM bilayers), in coexistence with β-sitosterol/milk-SM complexes in the L_o phase

(β-sitosterol rich bilayers). These results obtained with β-sitosterol in milk-SM bilayers are in agreement with the role played by cholesterol in phospholipid bilayers (Jovanović et al., 2018), and SM bilayers (Chemin et al., 2008) including milk-SM bilayers (Lopez et al., 2018).

Interestingly, the presence of β-sitosterol molecules induced an increase in the thickness of the bilayers in the ordered phase (10 °C) from 73.6 Å (milk-SM alone) to 76 Å. Furthermore, the 3D representation of the XRD patterns recorded at small angles showed a stabilisation of the lamellar organisation towards higher temperatures in presence of β-sitosterol as compared to milk-SM alone before phase transition occured, and a quite linear evolution of the lamellar organisation without structural reorganisations in the gel phase (**Fig 5**). We interpreted that β-sitosterol molecules inserted the milk-SM bilayers along the acyl chains, induced an increase in the bilayer thickness due to the length of β-sitosterol molecules and β-sitosterol – SM interactions, and prevented the gel phase polymorphism from the fully interdigitated ($L_{\beta 1}$) lamellar gel phase to the mixed interdigitated ($L_{\beta 2}$) lamellar gel phase. The XRD results also showed an increase in the thickness of the bilayers in the fluid state in presence of β-sitosterol compared to bilayers composed of milk-SM alone (from 67.7 to 73.5 Å) associated with a decrease in the MHPW from 0.01430 $Å^{-1}$ (0 %mol β-sitosterol) to 0.00634 $Å^{-1}$ (25 %mol β-sitosterol), indicating an increased order of the milk-SM chains induced by the presence of β-sitosterol molecules.

With 40 %mol β-sitosterol in the samples, a series of sharp reflections were recorded at wide angles, superimposed on the diffuse 4.6 Å scatter arising from the fatty acid packing in the L_o phase (**Fig 4 B**). These Bragg spacings were attributed to β-sitosterol crystals. The comparison of these Bragg spacings with those recorded in the anhydrous β-sitosterol powder indicated that, in the milk-SM/β-sitosterol samples (60/40 %mol), the β-sitosterol crystals were in an hydrated state (**Fig 4 C**), as previously described in literature (Christiansen et al., 2002). CLSM observations revealed the presence of β-sistosterol microcrystals in the samples containing 40 %mol β-sitosterol (**Fig 4 C, inset**). We therefore interpreted that the β-sitosterol molecules were no longer completely solubilised by the milk-SM bilayers, and that sterol-sterol van der Waals interactions occured resulting in the formation of high-melting point β-sitosterol crystals in the aqueous phase surrounding the milk-SM/β-sitosterol sphingosomes.

3.2.3. Molecular interactions between milk-SM and β-sitosterol in monolayers spread at the buffer/air interface

In this part of the work, the molecular interactions between milk-SM and β-sitosterol molecules were studied with the Langmuir monolayer technique. Milk-SM, β-sitosterol and milk-SM/ β-sitosterol mixtures were spread over the PIPES buffer surface to form monolayers at the PIPES buffer/air interface. **Figure 6** shows representative surface pressure (π) – area (A) isotherms that have been recorded at 20 °C for milk-SM, β-sitosterol and the mixed systems characterised by different molar ratios $X_{\beta\text{-sitosterol}}/(1\text{-}X)_{\text{milk-SM}}$. For the β-sitosterol monolayers ($X_{\beta\text{-sitosterol}} = 1$), the surface pressure of the π - A curve sharply increased at area 43 $Å^2$/molecule. This result showed that β-sitosterol molecules were in a solid phase during the compression, in relation to the planar and rigid structure of the molecule (**Fig. 1**A), and was in line with the literature (Hac-Wydro and Dynarowicz-Łatka, 2008). For the milk-SM monolayers ($X_{\beta\text{-sitosterol}} = 0$), the surface pressure of the π - A curves increased at area 82 $Å^2$/molecule. This value was in accordance with previous reports on milk-SM monolayers (Cheng et al., 2017; Obeid et al., 2019). The increase in the surface pressure recorded during compression was not continuous, but exhibited changes in the the π - A curve slope. As previously reported for milk-SM (Cheng et al., 2017; Obeid et al., 2019), the changes characterized for π = 10 mN/m corresponded to a pressure-induced and two-dimensional phase transition between a liquid expanded (LE ; low pressures) phase and a liquid condensed (LC ; high pressures) phase. At 20 °C and depending on surface pressure, the milk-SM molecules spread out in monolayers can therefore exist in the LE or the LC phase. According to literature, the LE state is characterized by a fluid and disordered organization of the acyl chains in which only the polar groups are constrained to be in contact with the sub-phase, whereas the LC phase is characterized by an organization of the acyl chains in an ordered crystalline sub-cell since the molecules are arranged near to their closest possible packing (Gaines, 1966). In the LC phase, the milk-SM molecules can hardly be further compacted which explains why the slope of the π - A curve is higher than in the LE phase, as previously reported (Cheng et al., 2017; Obeid et al., 2019).

The presence and the increased proportion of β-sitosterol into the milk-SM monolayers affected the position and the shape of the π - A curves (**Fig 6**). The transition from the LC to the LE phase was not present for $X_{\beta\text{-sitosterol}} > 0.05$. The π - A curves of the mixed monolayers became steeper with the increase of β-sitosterol content in the monolayers in comparison to the π - A

curves of the milk-SM. In addition, the π - A curves shifted in position towards lower mean molecular areas and started to resemble the isotherm recorded for β-sitosterol ($X_{\beta\text{-sitosterol}} = 1$).

The plots of the mean area per molecule (A_{12}) *versus* β-sitosterol molar fraction in the films ($X_{\beta\text{-sitosterol}}$) permitted the determination of molecular interactions between milk-SM molecules and β-sitosterol molecules in the mixed monolayers. The plots were prepared at two different surface pressures, π = 10 mN/m and π = 25 mN/m that correspond to surface pressures for which milk-SM is in the LE state and in the LC state respectively. Moreover, π = 25 mN/m is presumed to be the one prevailing within biological membranes (Marsh, 1996). **Figure 6-B** shows the plot of ideal mixing (A_{12} Ideal-mix dashed lines) and A_{12} values as a function of film composition (solid lines). Except for $X_{\beta\text{-sitosterol}} = 0.05$, negative deviations from the ideal behaviour were observed for all the film compositions that have been investigated. This corresponds to a decrease of the surface area occupied by molecules in the monolayer at the PIPES buffer/air interface and indicated that mixed milk-SM/β-sitosterol films were more condensed than ideal ones. These results suggested that the interactions between milk-SM molecules and β-sitosterol molecules in their mixed films were more attractive than the milk-SM/milk-SM and β-sitosterol/β-sitosterol intermolecular van der Waals forces in the respective single component films. The cross-sectional surface area of β-sitosterol molecules is highly sensitive to changes in surface pressure. Then, the experimentally observed changes in the areas of mixed milk-SM/β-sitosterol films can be attributed almost exclusively to configurational changes of milk-SM, i.e. ordering that β-sitosterol imparts to the milk-SM molecules. These experiments revealed that β-sitosterol induced an interfacial area condensation of the milk-SM molecules, revealing its ‘‘condensing effect”, as previously reported for cholesterol in mixed milk-SM/cholesterol monolayers (Cheng et al., 2017). This was interpreted as a consequence of a beneficial separation of milk-SM molecules by β-sitosterol that was attributed to attractive interactions between the NH group of SM molecules and the OH group of β-sitosterol (hydrogen bonding), and to the decrease of the electrostatic forces existing between polar groups of milk-SM molecules, as already discussed for cholesterol and SM (Hac-Wydro and Dynarowicz-Łatka, 2008; Smaby et al., 1994). Our results are in agreement with the condensing effect reported for β-sitosterol on egg-SM monolayers (Hac-Wydro and Dynarowicz-Łatka, 2008).

3.2.4. The incorporation of sterol molecules in milk-SM bilayers affects the morphology of the sphingosomes

The microstructure of milk-SM/sterol samples including the morphology of milk-SM sphingosomes in presence of sterols (β-sitosterol or cholesterol) was examined by confocal microscopy combined with DIC (**Fig 7**).

The sphingosomes composed of milk-SM corresponded to multilamellar vesicles with a spherical and facetted morphology (**Fig 7-A**) due to the gel phase of milk-SM at 19 °C (**Fig 4 and 5**), in agreement with our previous study (Lopez et al., 2022).

Milk-SM sphingosomes loaded with β-sitosterol exhibited changes in their morphology towards elongated structures. Facetted sphingosomes were observed in presence of 10 %mol and 20 %mol β-sitosterol in the samples (**Fig 7 B & C**). For 20 %mol β-sitosterol in the samples, the coexistence of spherical facetted sphingosomes with elongated sphingosomes was observed, and interpreted as the coexistence of milk-SM bilayers in the gel and L_o phases, respectively (**Fig 7-C**), in agreement with XRD results (**Fig 4**). For a molar fraction of 30 %mol β-sitosterol, most of the sphingosomes were elongated and the spherical sphingosomes were non-facetted (**Fig 7-D**). CLSM images revealed the formation of β-sitosterol microcrystals for 40 %mol β-sitosterol in the samples, which indicated a partitioning of β-sitosterol molecules between the milk-SM bilayers and the aqueous phase (**Fig 7-E**). The presence of β-sitosterol microcrystals was in agreement with their XRD signature recorded for milk-SM/β-sitosterol 60/40 %mol samples (**Fig 4**).

For comparison with the results obtained with milk-SM/β-sitosterol samples, and to complete our previous works dedicated to the elucidation of the functional role of cholesterol on milk-SM membranes (Cheng et al., 2017; Et-Thakafy et al., 2019; Lopez et al., 2018, 2010; Murthy et al., 2015), the microstructure of milk-SM/cholesterol sphingosomes was examined by confocal microscopy combined with DIC (**Fig 8**). As expected, the milk-SM sphingosomes observed at 19 °C corresponded to spherical and facetted vesicles in accordance with the gel phase of the milk-SM bilayers. The addition of cholesterol induced in increase in the size of the sphingosomes and the formation of elongated sphingosomes. The attractive molecular interactions between milk-SM and cholesterol that induce i) a condensing effect by the area occupied per phospholipid (Cheng et al., 2017), ii) an ordering effect through blocking the lateral arrangement into L_o phase (Lopez et al., 2018) and iii) a softening effect by decreasing the Young modulus of the milk-SM membrane (Et-Thakafy et al., 2019), also lead to membrane

fusion with changes in the morphology of the sphingosomes from spherical to elongated shapes (**Fig 8**).

Altogether, the microscopic observations performed with milk-SM/β-sitosterol and milk-SM/cholesterol multilamellar vesicles revealed that both sterol molecules induced changes in the morphology of the sphingosomes from facetted spherical to elongated shapes. These resuts showed that the sterols incorporated the host milk-SM bilayer membranes, modulated the bilayer structure (from gel to L_o phase) and properties (softening of the membranes), changed the intrinsic curvature of the milk-SM bilayers and induced membrane fusion. Such changes in the morphology of milk-SM sphingosomes towards elongated shapes in presence of guest molecules has been previously reported for α-tocopherol (Lopez et al., 2022), and has been discussed for cholesterol in biological and model membranes (Yang et al., 2016).

3.3. Towards food applications : Solubilisation of β-sitosterol molecules within milk-SM containing polar lipid vesicles

In this part of the work, we examined the capacity of a natural mixture of milk polar lipids recovered from the bovine MFGM to incorporate β-sitosterol molecules within membrane vesicles for their solubilisation (**Fig 9**). The milk polar lipid mixture contained 38.7 %wt milk-SM that exhibit attractive interactions with β-sitosterol molecules (**Fig 6**), and additional anionic and zwitterionic phospholipids from the MFGM (**Fig 1**).

On heating, fully hydrated milk polar lipid vesicles exhibited a broad and multicomponent endothermic signal ranging from 5 to 41.5 °C with T_m = 35.7 ± 0.2 °C (**Fig 9 A**), in accordance with previous results (Murthy et al., 2015). This broad endotherm resulted from the complex composition of milk polar lipids from the MFGM (various polar lipid species including milk-SM, PC, PE, PI, PS with saturated and unsaturated acyl chains). The complex MFGM polar lipid mixture exhibited a T_m close to the T_m of the milk-SM (T_m milk-SM = 34.5 ± 0.3 °C ; **Fig 3**) in coherence with its relative proportions in the milk polar lipid extract, i.e. 38.7 %wt. The addition of β-sitosterol affected the properties of the milk polar lipid bilayers with a decrease in the whole enthalpy of melting ΔH_m (**Fig 9 B**) and a decrease in the temperature of melting T_m to 26.2 ± 0.6 °C in presence of 19.4 %wt (30.5 %mol) β-sitosterol in the bilayers (**Fig 9 C**). In presence of 19.4 %wt β-sitosterol, the DSC thermogram exhibited 3 endotherms successively recorded as a function of temperature on heating and the phase transition characterised by T_m

was not fully abolished (**Fig 9A**). Whatever the β-sitosterol concentration, the endotherm recorded by DSC on heating, that corresponds to the gel - L_α phase transition of milk polar lipid bilayers including milk-SM was reversible upon cooling and immediate reheating (results not shown). This means that changes in the physical state of milk polar lipid bilayers did not induce a discharge of β-sitosterol molecules outside the vesicles.

XRD experiments showed that milk polar lipids formed lamellar structures whatever the temperature, characterised by thicknesses of d = 77.2 Å (T=10°C < T_m) and d = 68.6 Å (T=60°C > T_m) (**Fig 9D**). At 10°C, the recording at wide angles of a single diffraction line located at q= 1.5077 $Å^{-1}$ (d = 4.17 Å) was characteristic of the hexagonal packing of the fatty acid chains in the gel phase formed by the saturated high T_m polar lipids below their melting temperature, e.g. milk-SM, DPPC, POPE (Murthy et al., 2015). This gel phase was in coexistence with a L_α phase formed by the unsaturated polar lipids. At 60°C, all the polar lipids were in the L_α phase, as previously reported (Murthy et al., 2015). The addition of β-sitosterol induced a decrease in the proportion of the gel phase and the formation of a L_o phase. The residual gel phase recorded with 19.4 %wt β-sitosterol was in agreement with the presence of the endotherm recorded by DSC and corresponding to the gel to L_α phase transition characterised by T_m (**Fig 9A**). The formation of L_o phase within milk polar lipids was previosuly evidenced by XRD in presence of cholesterol (Murthy et al., 2016). In the complex mixture of milk polar lipids, β-sitosterol molecules may partition between the milk-SM molecules (formation of the L_o phase with attractive molecular interactions between milk-SM and β-sitosterol) and the unsaturated phospholipids that form a fluid matrix.

The microscopic observations of the samples revealed the formation of spherical milk polar lipid vesicles in absence of β-sitosterol, and elongated structures in presence of 19.4 %wt β-sitosterol that resulted from membrane fusion (**Fig 9E**). We did not observe the formation of β-sitosterol microcrystals in the samples. The changes in the morphology of the milk polar lipid vesicules was in agreement with the formation of elongated milk-SM sphingosomes in presence of sterols, both β-sitosterol and cholesterol (**Figs 7 and 8**).

As a conclusion, we showed that β-sitosterol molecules successfully integrated the host membrane of milk polar lipids, intercalated between individual polar lipids and hypothesised specific attractive interactions with milk-SM, as previously reported for cholesterol (Murthy et al., 2015). The solubilisation of up to 20 %wt β-sitosterol within milk polar lipid vesicles was efficient without the detection of microscrystals in the surrounding aqueous phase.

3.4. General discussion : from molecular explanations to food applications

SM molecules and other milk polar lipids (PC, PE, PI, PS) have fairly cylindrical molecular shapes, making them form bilayers when hydrated to minimise free energies (Marsh, 2013) ; they are therefore able to form vesicles under shear. In this study, we showed by the combination of biophysical techniques that β-sitosterol molecules i) are able to integrate into milk-SM and milk polar lipid membranes, ii) determine the physical properties of these membranes, and iii) induce changes in the morphology of the vesicles through changes in the membrane curvature and membrane fusion. The solubilisation and the effects of plant sterols such as β-sitosterol molecules on milk-SM and milk polar lipid membrane properties result from the structure of these plant compounds. β-sitosterol molecules are amphiphilic molecules having a large nonpolar lipophilic steroidal structure containing a hydrophobic steroid planar ring system with a flexible side tail at carbon 17 and a β-hydroxyl polar head (**Fig 1 A**). Free plant sterols such as β-sitosterol fit in membranes, because the overall length of free plant sterols is virtually the same as that of a phospholipid monolayer, i.e. 2.1 nm. The use of milk-SM molecules that contain saturated long acyl chains (**Fig 1 C**) was particularly interesting since i) the hydrocarbon chain composition of the host bilayer governs the hydrophobic length of the lipid molecule and impacts the thickness of the host bilayer in which the β-sitosterol molecules can extend, and ii) these saturated chains can contribute to the protection of plant sterols towards oxidation as compared to unsaturated glycerophospolipids (DOPC, POPC). Moreover, β-sitosterol molecules could be solubilised within milk-SM bilayers together with the lipophilic antioxiant tocopherols (Lopez et al., 2022) for an optimized protection against oxidation.

In a bilayer of glycerophospholipids or SM, the β-hydroxyl polar group of the sterol molecule aligns and interacts with the hydrophilic head group of phospholipids facing the aqueous phase, i.e. with the ester carbonyl groups of the glycerophospholipids and also with the hydroxyl group of the sphingosine base of SM. Furthermore, the amide carbonyl group in SM can act as hydrogen acceptor and gives SMs the unique ability to form intermolecular hydrogen bonding with the hydroxyl group of sterols such as β-sitosterol (Ramstedt and Slotte, 2002). The hydrogen bonding to the polar headgroup and interfacial regions of the host lipid bilayer is of considerable importance, especially in the SM (McMullen and McElhaney, 1996; McMullen et al., 2004; Ramstedt and Slotte, 2002). The hydrophobic part of the sterol molecule extends into

the hydophobic core of the lipid bilayer and is oriented parallel to the acyl chains of glycerophospholipids and sphingolipids, as discussed for cholesterol (Yeagle, 1985). The influence of β-sitosterol on the sphingosome membranes results from the attractive molecular interactions between β-sitosterol and milk-SM interactions as examined in this study by the Langmuir technique (**Fig 6**). The condensing effect of β-sitosterol on milk-SM films was attributed to the formation of stable complexes of specific stoichiometry between interacting molecules. These interactions involve the forces between β-sitosterol hydroxyl group and polar heads of SM as well as the attractive van der Waals interactions between the hydrophobic part of β-sitosterol molecule and the saturated long chains of SM (Israelachvili, 2011). The sterols create planar surfaces at both the top and the bottom of the molecules, which allow for multiple hydrophobic interactions between the rigid sterol nucleus and the membrane matrix (Bloch, 1983). The additional carbons at C-24 in the side chain of β-sitosterol compared to cholesterol increase the hydrophobicity of β-sitosterol molecules (Piironen et al., 2000) and may favor their interactions with the hydrocarbon chains of SM molecules within the bilayer membranes of the sphingosomes. In presence of β-sitosterol, a higher degree of conformational order is imposed on the acyl tails of milk-SM molecules by the rigid ring structure of β-sitosterol increasing the thickness of the lipid bilayer and the packing of molecules, although lipids remain laterally mobile, as characterized by XRD (**Fig 4 and 5**).

In this study, we showed that 30 - 35 %mol (18.2 – 21.8 %wt) β-sitosterol can be incorporated into milk-SM membranes, and that at least 20 %wt β-sitosterol can be incorporated into milk polar lipid membranes whithout the formation of β-sitosterol microcrystals in the aqueous phase. These results open perspectives for the utilisation of milk polar lipids for the solubilisation of plant sterols such as β-sitosterol into functional foods. Milk polar lipids can be prepared from by-products of the dairy industry (buttermilk, butter serum, cheese whey) ; powdered ingredients enriched in milk polar lipids are currently commercially available in the worldwide market (Fontecha et al., 2020; Lopez et al., 2019). In order to provide 2g/day β-sitosterol (Gylling et al., 2014), a food product containing 10 %wt lipids (2 g β-sitosterol + 8 g milk polar lipids) should be prepared. The consumption of 100 g of this preparation per day could be recommended as primary dietary prevention to reduce the risk of cardiovascular disease in adult consumers. This food system could be, for example, spreads or dairy-based

products such as portions of cream cheese. Clinical research studies are required to evaluate the benefits of free β-sitosterol solubilised in milk-SM based sphingosomes.

Concerning the dietary intake of plant sterols, it is important to precise the population (newborns, infants, adults) since their positive impact on human health has been proven after supplementation in adults and in the treatment of dislipidemia in children and adolescents (Mantovani and Pugliese, 2021). The attractive interactions between plant sterols such as β-sitosterol and milk-SM raise the question of their functions in newborns that consume infant milk formulas enriched in milk-SM from the bovine MFGM and that also contain plant sterols originating from the vegetable oils used in the formulation (Claumarchirant et al., 2016, 2015). Further research studies are required to evaluate the role of milk-SM / plant sterol complexes on the absorption of cholesterol in infants.

4. Conclusions

In this study, we showed that milk-SM molecules organised as sphingosomes and milk polar lipids organised as vesicles can successfully solubilise free β-sitosterol molecules in their bilayers due to adapted structural features and attractive molecular interactions. We also showed, by using the combination of biophysical techniques, that β-sitosterol molecules modulate the bilayer structure and properties in multiple ways and the morphology of the vesicles. We conclude that the milk-SM containing vesicles are promising lipid carriers to solubilise free plant sterols such as β-sitosterol molecules and that they hold a strong potential for the developement of plant sterol enriched functional foods. In addition, an innovative co-formulation of the antioxidant tocopherols along with plant sterols within sphingosomes could enhance oxidative stability of plant sterols. In perspective, it appears important to conduct *in vitro* and *in vivo* studies to assess the effectiveness of SM-based vesicles loaded with plant sterols in fortified foods.

Acknowledgements

The authors thank synchrotron Soleil for allocating beam time on the SWING beamline (main proposer C. Lopez). C. Lopez thanks B. Novales from INRAE, PROBE Research Infrastructure and BIBS facility (BIA research unit, Nantes, France ; https://www.bibs.inrae.fr) where part of the CLSM observations was performed.

CRediT authorship contribution statement

Christelle Lopez: Conceptualization, Supervision, Writing & editing. **Elisabeth David-Briand**: Investigation. **Cristelle Mériadec**: Investigation. **Virginie Lollier** : Data analysis. **Thomas Bizien**: Investigation. **Javier Pérez** : Supervision. **Franck Artzner**: Conceptualization, Supervision, Writing & editing. All the authors contributed to manuscript writing and approved the submitted version.

Conflict of interest

The authors declare no conflict of interest

References

Acevedo, N.C., Franchetti, D., 2016. Analysis of co-crystallized free phytosterols with triacylglycerols as a functional food ingredient. Food Research International 85, 104–112. https://doi.org/10.1016/j.foodres.2016.04.012

Alemany, L., Barbera, R., Alegría, A., Laparra, J.M., 2014. Plant sterols from foods in inflammation and risk of cardiovascular disease: A real threat? Food and Chemical Toxicology 69, 140–149. https://doi.org/10.1016/j.fct.2014.03.038

Alexander, M., Acero Lopez, A., Fang, Y., Corredig, M., 2012. Incorporation of phytosterols in soy phospholipids nanoliposomes: Encapsulation efficiency and stability. LWT 47, 427–436. https://doi.org/10.1016/j.lwt.2012.01.041

American Heart Association Nutrition Committee, Lichtenstein, A.H., Appel, L.J., Brands, M., Carnethon, M., Daniels, S., Franch, H.A., Franklin, B., Kris-Etherton, P., Harris, W.S., Howard, B., Karanja, N., Lefevre, M., Rudel, L., Sacks, F., Van Horn, L., Winston, M., Wylie-Rosett, J., 2006. Diet and lifestyle recommendations revision 2006: a scientific statement from the American Heart Association Nutrition Committee. Circulation 114, 82–96. https://doi.org/10.1161/CIRCULATIONAHA.106.176158

Battacchi, D., Verkerk, R., Pellegrini, N., Fogliano, V., Steenbekkers, B., 2020. The state of the art of food ingredients' naturalness evaluation: A review of proposed approaches and their relation with consumer trends. Trends in Food Science & Technology 106, 434–444. https://doi.org/10.1016/j.tifs.2020.10.013

Berge, null, Konovalov, null, Lajzerowicz, null, Renault, null, Rieu, null, Vallade, null, Als-Nielsen, null, Grübel, null, Legrand, null, 1994. Melting of short 1-alcohol monolayers on water: Thermodynamics and x-ray scattering studies. Phys Rev Lett 73, 1652–1655. https://doi.org/10.1103/PhysRevLett.73.1652

Berger, A., Jones, P.J., Abumweis, S.S., 2004. Plant sterols: factors affecting their efficacy and safety as functional food ingredients. Lipids in Health and Disease 3, 5. https://doi.org/10.1186/1476-511X-3-5

Bezelgues, J.-B., Morgan, F., Palomo, G., Crosset-Perrotin, L., Ducret, P., 2009. Short communication: Milk fat globule membrane as a potential delivery system for liposoluble nutrients. Journal of Dairy Science 92, 2524–2528. https://doi.org/10.3168/jds.2008-1725

Bloch, K.E., 1983. Sterol, Structure and Membrane Function. Critical Reviews in Biochemistry 14, 47–92. https://doi.org/10.3109/10409238309102790

Bouzo, B.L., Lores, S., Jatal, R., Alijas, S., Alonso, M.J., Conejos-Sánchez, I., de la Fuente, M., 2021. Sphingomyelin nanosystems loaded with uroguanylin and etoposide for treating metastatic colorectal cancer. Sci Rep 11, 17213. https://doi.org/10.1038/s41598-021-96578-z

Chawla, R., S, S., Goel, N., 2016. PHYTOSTEROL AND ITS ESTERS AS NOVEL FOOD INGREDIENTS: A REVIEW. Asian Journal of Dairy and Food Research 35, 217–226.

Chemin, C., Bourgaux, C., Péan, J.-M., Pabst, G., Wüthrich, P., Couvreur, P., Ollivon, M., 2008. Consequences of ions and pH on the supramolecular organization of sphingomyelin and sphingomyelin/cholesterol bilayers. Chemistry and Physics of Lipids 153, 119–129. https://doi.org/10.1016/j.chemphyslip.2008.03.002

Cheng, K., Ropers, M.-H., Lopez, C., 2017. The miscibility of milk sphingomyelin and cholesterol is affected by temperature and surface pressure in mixed Langmuir monolayers. Food Chemistry 224, 114–123. https://doi.org/10.1016/j.foodchem.2016.12.035

Christiansen, L.I., Rantanen, J.T., von Bonsdorff, A.K., Karjalainen, M.A., Yliruusi, J.K., 2002. A novel method of producing a microcrystalline β-sitosterol suspension in oil. European Journal of Pharmaceutical Sciences 15, 261–269. https://doi.org/10.1016/S0928-0987(01)00223-8

Claumarchirant, L., Cilla, A., Matencio, E., Sanchez-Siles, L.M., Castro-Gomez, P., Fontecha, J., Alegría, A., Lagarda, M.J., 2016. Addition of milk fat globule membrane as an ingredient of infant formulas for resembling the polar lipids of human milk. International Dairy Journal 61, 228–238. https://doi.org/10.1016/j.idairyj.2016.06.005

Claumarchirant, L., Matencio, E., Sanchez-Siles, L.M., Alegría, A., Lagarda, M.J., 2015. Sterol Composition in Infant Formulas and Estimated Intake. J. Agric. Food Chem. 63, 7245–7251. https://doi.org/10.1021/acs.jafc.5b02647

Clifton, P., 2015. Influence of Food Matrix on Sterol and Stanol Activity. J AOAC Int 98, 677–678. https://doi.org/10.5740/jaoacint.SGEClifton

Cusack, L.K., Fernandez, M.L., Volek, J.S., 2013. The Food Matrix and Sterol Characteristics Affect the Plasma Cholesterol Lowering of Phytosterol/Phytostanol1. Adv Nutr 4, 633–643. https://doi.org/10.3945/an.113.004507

da Silva, M.G., de Godoi, K.R.R., Gigante, M.L., Cardoso, L.P., Ribeiro, A.P.B., 2022. Nanostructured lipid carriers for delivery of free phytosterols: Effect of lipid composition and chemical interesterification on physical stability. Colloids and Surfaces A: Physicochemical and Engineering Aspects 640, 128425. https://doi.org/10.1016/j.colsurfa.2022.128425

David, G., Pérez, J., 2009. Combined sampler robot and high-performance liquid chromatography: a fully automated system for biological small-angle X-ray scattering experiments at the Synchrotron SOLEIL SWING beamline. J Appl Cryst 42, 892–900. https://doi.org/10.1107/S0021889809029288

Engel, R., Schubert, H., 2005. Formulation of phytosterols in emulsions for increased dose response in functional foods. Innovative Food Science & Emerging Technologies 6, 233–237. https://doi.org/10.1016/j.ifset.2005.01.004

Et-Thakafy, O., Guyomarc'h, F., Lopez, C., 2019. Young modulus of supported lipid membranes containing milk sphingomyelin in the gel, fluid or liquid-ordered phase, determined using AFM force spectroscopy. Biochimica et Biophysica Acta (BBA) - Biomembranes 1861, 1523–1532. https://doi.org/10.1016/j.bbamem.2019.07.005

Expert Panel on Detection, Evaluation, and Treatment of High Blood Cholesterol, 2001. Executive Summary of the Third Report of the National Cholesterol Education Program (NCEP) Expert Panel on Detection, Evaluation, and Treatment of High Blood Cholesterol in Adults (Adult Treatment Panel III). JAMA 285, 2486–2497. https://doi.org/10.1001/jama.285.19.2486

Farhang, B., Kakuda, Y., Corredig, M., 2012. Encapsulation of ascorbic acid in liposomes prepared with milk fat globule membrane-derived phospholipids. Dairy Sci. & Technol. 92, 353–366. https://doi.org/10.1007/s13594-012-0072-7

Feng, S., Belwal, T., Li, L., Limwachiranon, J., Liu, X., Luo, Z., 2020. Phytosterols and their derivatives: Potential health-promoting uses against lipid metabolism and associated diseases, mechanism, and safety issues. Comprehensive Reviews in Food Science and Food Safety 19, 1243–1267. https://doi.org/10.1111/1541-4337.12560

Filippov, A., Oradd, G., Lindblom, G., 2006. Sphingomyelin structure influences the lateral diffusion and raft formation in lipid bilayers. Biophys. J. 90, 2086–2092. https://doi.org/10.1529/biophysj.105.075150

Fontecha, J., Brink, L., Wu, S., Pouliot, Y., Visioli, F., Jiménez-Flores, R., 2020. Sources, Production, and Clinical Treatments of Milk Fat Globule Membrane for Infant Nutrition and Well-Being. Nutrients 12. https://doi.org/10.3390/nu12061607

Gaines, G.L., 1966. Insoluble monolayers at liquid-gas interfaces. Interscience Publishers.

Grundy, S.M., Arai, H., Barter, P., Bersot, T.P., Betteridge, D.J., Carmena, R., Cuevas, A., Davidson, M.H., Genest, J., Kesäniemi, Y.A., Sadikot, S., Santos, R.D., Susekov, A.V., Sy, R.G., LaleTokgözoglu, S., Watts, G.F., Zhao, D., 2014. An International Atherosclerosis Society Position Paper: Global recommendations for the management of dyslipidemia-Full report. Journal of Clinical Lipidology 8, 29–60. https://doi.org/10.1016/j.jacl.2013.12.005

Gülseren, I., Corredig, M., 2013. Storage Stability and Physical Characteristics of Tea-Polyphenol-Bearing Nanoliposomes Prepared with Milk Fat Globule Membrane Phospholipids. J. Agric. Food Chem. 61, 3242–3251. https://doi.org/10.1021/jf3045439

Guner, S., Oztop, M.H., 2017. Food grade liposome systems: Effect of solvent, homogenization types and storage conditions on oxidative and physical stability. Colloids and Surfaces A: Physicochemical and Engineering Aspects 513, 468–478. https://doi.org/10.1016/j.colsurfa.2016.11.022

Gylling, H., Plat, J., Turley, S., Ginsberg, H.N., Ellegård, L., Jessup, W., Jones, P.J., Lütjohann, D., Maerz, W., Masana, L., Silbernagel, G., Staels, B., Borén, J., Catapano, A.L., De Backer, G., Deanfield, J., Descamps, O.S., Kovanen, P.T., Riccardi, G., Tokgözoglu, L., Chapman, M.J., 2014. Plant sterols and plant stanols in the management of dyslipidaemia and prevention of cardiovascular disease. Atherosclerosis 232, 346–360. https://doi.org/10.1016/j.atherosclerosis.2013.11.043

Hac-Wydro, K., Dynarowicz-Łatka, P., 2008. The impact of sterol structure on the interactions with sphingomyelin in mixed langmuir monolayers. J Phys Chem B 112, 11324–11332. https://doi.org/10.1021/jp803193s

Halling, K.K., Slotte, J.P., 2004. Membrane properties of plant sterols in phospholipid bilayers as determined by differential scanning calorimetry, resonance energy transfer and detergent-induced solubilization. Biochimica et Biophysica Acta (BBA) - Biomembranes 1664, 161–171. https://doi.org/10.1016/j.bbamem.2004.05.006

Israelachvili, J., 2011. Intermolecular and Surface Forces - 3rd Edition. Elsevier.

Izadi, Z., Nasirpour, A., Garousi, G., 2012. Optimization of Phytosterols Dispersion in an Oil/Water Emulsion Using Mixture Design Approach. Journal of Dispersion Science and Technology 33, 1715–1722. https://doi.org/10.1080/01932691.2011.646599

Jatal, R., Mendes Saraiva, S., Vázquez-Vázquez, C., Lelievre, E., Coqueret, O., López-López, R., de la Fuente, M., 2022. Sphingomyelin nanosystems decorated with TSP-1 derived peptide targeting senescent cells. Int J Pharm 617, 121618. https://doi.org/10.1016/j.ijpharm.2022.121618

Jesch, E.D., Carr, T.P., 2017. Food Ingredients That Inhibit Cholesterol Absorption. Prev Nutr Food Sci 22, 67–80. https://doi.org/10.3746/pnf.2017.22.2.67

Jovanović, A.A., Balanč, B.D., Ota, A., Ahlin Grabnar, P., Djordjević, V.B., Šavikin, K.P., Bugarski, B.M., Nedović, V.A., Poklar Ulrih, N., 2018. Comparative Effects of Cholesterol and β-Sitosterol on

the Liposome Membrane Characteristics. European Journal of Lipid Science and Technology 120, 1800039. https://doi.org/10.1002/ejlt.201800039

Katan, M.B., Grundy, S.M., Jones, P., Law, M., Miettinen, T., Paoletti, R., 2003. Efficacy and Safety of Plant Stanols and Sterols in the Management of Blood Cholesterol Levels. Mayo Clinic Proceedings 78, 965–978. https://doi.org/10.4065/78.8.965

Kritchevsky, D., Chen, S.C., 2005. Phytosterols—health benefits and potential concerns: a review. Nutrition Research 25, 413–428. https://doi.org/10.1016/j.nutres.2005.02.003

Lagarda, M.J., García-Llatas, G., Farré, R., 2006. Analysis of phytosterols in foods. Journal of Pharmaceutical and Biomedical Analysis, Nutraceuticals Analysis 41, 1486–1496. https://doi.org/10.1016/j.jpba.2006.02.052

Law, M., 2000. Plant sterol and stanol margarines and health 320, 4.

Lopez, C., 2021. Valorization of dairy by-products for functional and nutritional applications: recent trends toward the milk fat globule membrane, in: Valorization of Agri-Food Wastes and By-Products - 1st Edition. Ed. Rajeev Bhat, pp. 415–424.

Lopez, C., 2020. Structure of the Milk Fat Globule Membrane: New Scientific Advances Revealing the Role of Sphingomyelin in Topographical and Mechanical Heterogeneities. Dairy Fat Products and Functionality 41–66. https://doi.org/10.1007/978-3-030-41661-4_3

Lopez, C., Blot, M., Briard-Bion, V., Cirié, C., Graulet, B., 2017. Butter serums and buttermilks as sources of bioactive lipids from the milk fat globule membrane: Differences in their lipid composition and potentialities of cow diet to increase n-3 PUFA. Food Research International 100, 864–872. https://doi.org/10.1016/j.foodres.2017.08.016

Lopez, C., Cauty, C., Guyomarc'h, F., 2019. Unraveling the Complexity of Milk Fat Globules to Tailor Bioinspired Emulsions Providing Health Benefits: The Key Role Played by the Biological Membrane. Eur. J. Lipid Sci. Technol. 121, 1800201. https://doi.org/10.1002/ejlt.201800201

Lopez, C., Cheng, K., Perez, J., 2018. Thermotropic phase behavior of milk sphingomyelin and role of cholesterol in the formation of the liquid ordered phase examined using SR-XRD and DSC. Chemistry and Physics of Lipids 215, 46–55. https://doi.org/10.1016/j.chemphyslip.2018.07.008

Lopez, C., David-Briand, E., Mériadec, C., Bourgaux, C., Pérez, J., Artzner, F., 2022. Milk sphingosomes as lipid carriers for tocopherols in aqueous foods: Thermotropic phase behaviour and morphology. Food Research International 162, 112115. https://doi.org/10.1016/j.foodres.2022.112115

Lopez, C., Madec, M.-N., Jiménez-Flores, R., 2010. Lipid Rafts in the Bovine Milk Fat Globule Membrane Revealed by the Lateral Segregation of Phospholipids and Heterogeneous Distribution of Glycoproteins. Food Chemistry 120, 22–33. https://doi.org/10.1016/j.foodchem.2009.09.065

Lopez, C., Mériadec, C., David-Briand, E., Dupont, A., Bizien, T., Artzner, F., Riaublanc, A., Anton, M., 2020. Loading of lutein in egg-sphingomyelin vesicles as lipid carriers: Thermotropic phase behaviour, structure of sphingosome membranes and lutein crystals. Food Research International 138, 109770. https://doi.org/10.1016/j.foodres.2020.109770

Mantovani, L.M., Pugliese, C., 2021. Phytosterol supplementation in the treatment of dyslipidemia in children and adolescents: a systematic review. Rev. paul. pediatr. 39, e2019389. https://doi.org/10.1590/1984-0462/2021/39/2019389

Marsh, D., 2013. Handbook of Lipid Bilayers, $ {number}nd édition. ed. CRC Press, Boca Raton, FL.

Marsh, D., 1996. Lateral pressure in membranes. Biochimica et Biophysica Acta (BBA) - Reviews on Biomembranes 1286, 183–223. https://doi.org/10.1016/S0304-4157(96)00009-3

Mattson, F.H., Grundy, S.M., Crouse, J.R., 1982. Optimizing the effect of plant sterols on cholesterol absorption in man. The American Journal of Clinical Nutrition 35, 697–700. https://doi.org/10.1093/ajcn/35.4.697

McClements, D.J., 2015. Nanoscale Nutrient Delivery Systems for Food Applications: Improving Bioactive Dispersibility, Stability, and Bioavailability. Journal of Food Science 80, N1602–N1611. https://doi.org/10.1111/1750-3841.12919

McKersie, B.D., Thompson, J.E., 1979. Influence of Plant Sterols on the Phase Properties of Phospholipid Bilayers. Plant Physiology 63, 802–805. https://doi.org/10.1104/pp.63.5.802

McMullen, T.P., McElhaney, R.N., 1996. Physical studies of cholesterol-phospholipid interactions. Current Opinion in Colloid & Interface Science 1, 83–90. https://doi.org/10.1016/S1359-0294(96)80048-3

McMullen, T.P.W., Lewis, R., McElhaney, R.N., 2004. Cholesterol-phospholipid interactions, the liquid-ordered phase and lipid rafts in model and biological membranes. Curr. Opin. Colloid Interface Sci. 8, 459–468. https://doi.org/10.1016/j.cocis.2004.01.007

Moreau, R.A., Nyström, L., Whitaker, B.D., Winkler-Moser, J.K., Baer, D.J., Gebauer, S.K., Hicks, K.B., 2018. Phytosterols and their derivatives: Structural diversity, distribution, metabolism, analysis, and health-promoting uses. Progress in Lipid Research 70, 35–61. https://doi.org/10.1016/j.plipres.2018.04.001

Murthy, A.V.R., Guyomarc'h, F., Lopez, C., 2016. Cholesterol Decreases the Size and the Mechanical Resistance to Rupture of Sphingomyelin Rich Domains, in Lipid Bilayers Studied as a Model of the Milk Fat Globule Membrane. Langmuir 32, 6757–6765. https://doi.org/10.1021/acs.langmuir.6b01040

Murthy, A.V.R., Guyomarc'h, F., Paboeuf, G., Vié, V., Lopez, C., 2015. Cholesterol strongly affects the organization of lipid monolayers studied as models of the milk fat globule membrane: Condensing effect and change in the lipid domain morphology. Biochimica et Biophysica Acta (BBA) - Biomembranes 1848, 2308–2316. https://doi.org/10.1016/j.bbamem.2015.06.014

Musa-Veloso, K., Poon, T.H., Elliot, J.A., Chung, C., 2011. A comparison of the LDL-cholesterol lowering efficacy of plant stanols and plant sterols over a continuous dose range: Results of a meta-analysis of randomized, placebo-controlled trials. Prostaglandins, Leukotrienes and Essential Fatty Acids 85, 9–28. https://doi.org/10.1016/j.plefa.2011.02.001

Nagachinta, S., Bouzo, B.L., Vazquez-Rios, A.J., Lopez, R., Fuente, M. de la, 2020. Sphingomyelin-Based Nanosystems (SNs) for the Development of Anticancer miRNA Therapeutics. Pharmaceutics 12, E189. https://doi.org/10.3390/pharmaceutics12020189

Obeid, S., Guyomarc'h, F., David-Briand, E., Gaucheron, F., Riaublanc, A., Lopez, C., 2019. The phase and charge of milk polar lipid membrane bilayers govern their selective interactions with proteins as demonstrated with casein micelles. Journal of Colloid and Interface Science 534, 279–290. https://doi.org/10.1016/j.jcis.2018.09.033

Ostlund, R.E., 2002. Phytosterols in human nutrition. Annu. Rev. Nutr. 22, 533–549. https://doi.org/10.1146/annurev.nutr.22.020702.075220

Parraga-Martinez, I., López-Torres-Hidalgo, J.D., del Campo-del Campo, J.M., Galdón-Blesa, M.P., Precioso-Yáñez, J.C., Rabanales-Sotos, J., García-Reyes-Ramos, M., Andrés-Pretel, F., Navarro-Bravo, B., Lloret-Callejo, Á., 2015. Long-term Effects of Plant Stanols on the Lipid Profile of Patients With Hypercholesterolemia. A Randomized Clinical Trial. Rev Esp Cardiol 68, 665–671. https://doi.org/10.1016/j.rec.2014.07.035

Pavani, M., Singha, P., Dash, D.R., Asaithambi, N., Singh, S.K., 2022. Novel encapsulation approaches for phytosterols and their importance in food products: A review. Journal of Food Process Engineering 45, e14041. https://doi.org/10.1111/jfpe.14041

Piironen, V., Lindsay, D.G., Miettinen, T.A., Toivo, J., Lampi, A.-M., 2000. Plant sterols: biosynthesis, biological function and their importance to human nutrition. Journal of the Science of Food and Agriculture 80, 939–966. https://doi.org/10.1002/(SICI)1097-0010(20000515)80:7<939::AID-JSFA644>3.0.CO;2-C

Plat, J., Mackay, D., Baumgartner, S., Clifton, P.M., Gylling, H., Jones, P.J.H., 2012. Progress and prospective of plant sterol and plant stanol research: Report of the Maastricht meeting. Atherosclerosis 225, 521–533. https://doi.org/10.1016/j.atherosclerosis.2012.09.018

Ramstedt, B., Slotte, J.P., 2002. Membrane properties of sphingomyelins. FEBS Lett 531, 33–37. https://doi.org/10.1016/s0014-5793(02)03406-3

Ras, R.T., Geleijnse, J.M., Trautwein, E.A., 2014. LDL-cholesterol-lowering effect of plant sterols and stanols across different dose ranges: a meta-analysis of randomised controlled studies. British Journal of Nutrition 112, 214–219. https://doi.org/10.1017/S0007114514000750

Rocha, V.Z., Ras, R.T., Gagliardi, A.C., Mangili, L.C., Trautwein, E.A., Santos, R.D., 2016. Effects of phytosterols on markers of inflammation: A systematic review and meta-analysis. Atherosclerosis 248, 76–83. https://doi.org/10.1016/j.atherosclerosis.2016.01.035

Román, S., Sánchez-Siles, L.M., Siegrist, M., 2017. The importance of food naturalness for consumers: Results of a systematic review. Trends in Food Science & Technology 67, 44–57. https://doi.org/10.1016/j.tifs.2017.06.010

Rossi, L., Sacanna, S., Velikov, K.P., 2011. Cholesteric colloidal liquid crystals from phytosterol rod-like particles. Soft Matter 7, 64–67. https://doi.org/10.1039/C0SM00822B

Salo, P., Wester, I., 2005. Low-Fat Formulations of Plant Stanols and Sterols. The American Journal of Cardiology, Role of Plant Stanol Esters in Cholesterol Management: Enhancing the Efficacy of Diet and Statin Therapy 96, 51–54. https://doi.org/10.1016/j.amjcard.2005.03.021

Scholz, B., Guth, S., Engel, K.-H., Steinberg, P., 2015. Phytosterol oxidation products in enriched foods: Occurrence, exposure, and biological effects. Mol Nutr Food Res 59, 1339–1352. https://doi.org/10.1002/mnfr.201400922

Shaghaghi, M., Amir, Harding, S.V., Jones, P.J.H., 2014. Water dispersible plant sterol formulation shows improved effect on lipid profile compared to plant sterol esters. Journal of Functional Foods 6, 280–289. https://doi.org/10.1016/j.jff.2013.10.017

Shaw, K.P., Brooks, N.J., Clarke, J.A., Ces, O., Seddon, J.M., Law, R.V., 2012. Pressure-temperature phase behaviour of natural sphingomyelin extracts. Soft Matter 8, 1070–1078. https://doi.org/10.1039/c1sm06703f

Simons, K., Ikonen, E., 1997. Functional rafts in cell membranes. Nature 387, 569–572. https://doi.org/10.1038/42408

Singh, H., 2006. The milk fat globule membrane—A biophysical system for food applications. Current Opinion in Colloid & Interface Science 11, 154–163. https://doi.org/10.1016/j.cocis.2005.11.002

Slotte, J.P., 2016. The importance of hydrogen bonding in sphingomyelin's membrane interactions with co-lipids. Biochimica et Biophysica Acta (BBA) - Biomembranes 1858, 304–310. https://doi.org/10.1016/j.bbamem.2015.12.008

Smaby, J.M., Brockman, H.L., Brown, R.E., 1994. Cholesterol's Interfacial Interactions with Sphingomyelins and Phosphatidylcholines: Hydrocarbon Chain Structure Determines the Magnitude of Condensation. Biochemistry 33, 9135–9142.

Tai, K., Liu, F., He, X., Ma, P., Mao, L., Gao, Y., Yuan, F., 2018. The effect of sterol derivatives on properties of soybean and egg yolk lecithin liposomes: Stability, structure and membrane characteristics. Food Research International 109, 24–34. https://doi.org/10.1016/j.foodres.2018.04.014

Thompson, A.K., Couchoud, A., Singh, H., 2009. Comparison of hydrophobic and hydrophilic encapsulation using liposomes prepared from milk fat globule-derived phospholipids and soya phospholipids. Dairy Sci. Technol. 89, 99–113. https://doi.org/10.1051/dst/2008036

Tolve, R., Cela, N., Condelli, N., Di Cairano, M., Caruso, M.C., Galgano, F., 2020. Microencapsulation as a Tool for the Formulation of Functional Foods: The Phytosterols' Case Study. Foods 9, E470. https://doi.org/10.3390/foods9040470

Turini, E., Sarsale, M., Petri, D., Totaro, M., Lucenteforte, E., Tavoschi, L., Baggiani, A., 2022. Efficacy of Plant Sterol-Enriched Food for Primary Prevention and Treatment of Hypercholesterolemia: A Systematic Literature Review. Foods 11, 839. https://doi.org/10.3390/foods11060839

Vanhanen, H., Blomqvist, S., Ehnholm, C., Hyvönen, M., Jauhiainen, M., Torstila, I., Miettinen, T., 1993. Serum cholesterol, cholesterol precursors, and plant sterols in hypercholesterolemic subjects with different apoE phenotypes during dietary sitostanol ester treatment. Journal of Lipid Research 34, 1535–1544. https://doi.org/10.1016/S0022-2275(20)36946-7

Vesper, H., Schmelz, E.-M., Nikolova-Karakashian, M.N., Dillehay, D.L., Lynch, D.V., Merrill, A.H., 1999. Sphingolipids in Food and the Emerging Importance of Sphingolipids to Nutrition. J Nutr 129, 1239–1250. https://doi.org/10.1093/jn/129.7.1239

Wang, F.C., Acevedo, N., Marangoni, A.G., 2017. Encapsulation of phytosterols and phytosterol esters in liposomes made with soy phospholipids by high pressure homogenization. Food Funct. 8, 3964–3969. https://doi.org/10.1039/C7FO00905D

Wechtersbach, L., Poklar Ulrih, N., Cigić, B., 2012. Liposomal stabilization of ascorbic acid in model systems and in food matrices. LWT - Food Science and Technology 45, 43–49. https://doi.org/10.1016/j.lwt.2011.07.025

Weihrauch, J.L., Gardner, J.M., 1978. Sterol content of foods of plant origin. J Am Diet Assoc 73, 39–47.

Yang, F., Chen, G., 2022. The nutritional functions of dietary sphingomyelin and its applications in food. Front Nutr 9, 1002574. https://doi.org/10.3389/fnut.2022.1002574

Yang, S., Zhu, M., Wang, N., Cui, X., Xu, Q., Saleh, A.S.M., Duan, Y., Xiao, Z., 2018. Influence of Oil Type on Characteristics of β-Sitosterol and Stearic Acid Based Oleogel. Food Biophysics 13, 362–373. https://doi.org/10.1007/s11483-018-9542-7

Yang, S.-T., Kreutzberger, A.J.B., Lee, J., Kiessling, V., Tamm, L.K., 2016. The role of cholesterol in membrane fusion. Chem. Phys. Lipids 199, 136–143. https://doi.org/10.1016/j.chemphyslip.2016.05.003

Yeagle, P.L., 1985. Cholesterol and the cell membrane. Biochimica et Biophysica Acta (BBA) - Reviews on Biomembranes 822, 267–287. https://doi.org/10.1016/0304-4157(85)90011-5

Zychowski, L.M., Logan, A., Augustin, M.A., Kelly, A.L., Zabara, A., O'Mahony, J.A., Conn, C.E., Auty, M.A.E., 2016. Effect of Phytosterols on the Crystallization Behavior of Oil-in-Water Milk Fat Emulsions. J. Agric. Food Chem. 64, 6546–6554. https://doi.org/10.1021/acs.jafc.6b01722

Figure caption

Figure 1 : Chemical structures of (**A**) β-sitosterol, (**B**) cholesterol and (**C**) milk polar lipids including milk-sphingomyelin, and the glycerophospholipids phosphatidylcholine (PC), phosphatidylethanolamine (PE), phosphatidylserine (PS) and phosphatidylinositol (PI).

Figure 2 : Characterisation of the powdered β-sitosterol crystals. **(A)** Microscopy images, **(B)** X-ray diffraction (XRD) pattern recorded at 20°C, **(C)** thermograms recorded by differential scanning calorimetry (DSC) on heating and cooling at 10°C/min as indicated in the figure, **(D)** synchrotron radiation XRD patterns recorded as a function of temperature on heating of β-sitosterol crystals at 10 °C/min from 20 to 200 °C. Abreviation : q = scattering vector.

Figure 3 : Effect of β-sitosterol on the thermotropic phase behavior of milk-sphingomyelin (milk-SM) bilayers revealed using differential scanning calorimetry (DSC). **(A)** Thermograms recorded on heating at 2 °C/min of milk-SM/ β-sitosterol samples, with the molar fraction of β-sitosterol indicated in the figure. **(B)** Melting enthalpy ΔH_m as a function of β-sitosterol concentration. **(C)** Melting transition temperature T_m as a function of β-sitosterol concentration. **(D)** Thermograms successively recorded on heating, cooling and immediate reheating at 2°C/min of fully hydrated milk-SM / β-sitosterol bilayers with various molar ratios indicated in the figures.

Figure 4 : Structural behavior of milk-sphingomyelin (milk-SM) bilayers containing various concentrations of β-sitosterol examined at 12 °C (blue colour) and 60 °C (red colour) using XRD **(A)** at small angles (SAXS) and **(B)** at wide angles (WAXS) ; arrows indicate XRD signal from β-sitosterol crystals. **(C)** XRD patterns recorded for powdered β-sitosterol crystals and milk-SM / β-sitosterol (60/40 %mol) samples showing reflections from β-sitosterol crystals combined with microscopic images showing the β-sitosterol crystals in the aqueous phase of the samples. Abreviation : q = scattering vector.

Figure 5 : Thermotropic phase behaviour of fully hydrated milk-sphingomyelin (milk-SM) bilayers alone, milk-SM / β-sitosterol (90/10 %mol) and milk-SM / β-sitosterol (75/25 %mol) samples examined using synchrotron radiation X-ray diffraction as a function of temperature (SR-XRDT) on heating at 2 °C/min. Three-dimensional plots of the XRD patterns recorded as a function of temperature at small (SAXS, left) and wide (WAXS, right) angles. (*) detector default) ; Abreviation : q = scattering vector.

Figure 6 : Interfacial properties of milk-sphingomyelin (milk-SM) and molecular interactions with β-sitosterol investigated in mixed Langmuir monolayers at 20 °C. **(A)** the surface pressure – area (π-A) isotherms of mixed monolayers formed at the air / buffer interface by milk-SM and β-sitosterol, **(B)** The mean area per molecule (A_{12}) versus composition (X β-sitosterol) plots for mixed monolayers of milk-SM and cholesterol at different constant surface pressures as indicated in the figure.

Figure 7: Microscopy images showing milk-sphingomyelin (MSM) sphingosomes, MSM sphingosomes loaded with β-sitosterol and β-sitosterol crystals. Confocal laser scanning microscopy (CLSM) with the Nile red fluorescent dye to label the hydrophobic part of the MSM sphingosome bilayers (red colour). DIC images are in grey levels. Fig E is the superimposition of CLSM and DIC images.

Figure 8: Microscopy images showing milk-sphingomyelin (MSM) sphingosomes and MSM sphingosomes loaded with cholesterol. Confocal laser scanning microscopy (CLSM) with the Nile red fluorescent dye to label the hydrophobic part of the MSM sphingosome bilayers (red colour). DIC images are in grey levels. Fig A (left and middle) is the superimposition of CLSM and DIC images.

Figure 9 : Thermal properties, structural organization and morphology of milk polar lipid vesicles containing various amounts of β-sitosterol. **(A)** Thermograms recorded by differential scanning calorimetry on heating of the samples at 2 °C/min, **(B)** Enthalpy of melting ΔH_m as a function of the amount of β-sitosterol, **(C)** Temperature of melting T_m as a function of the amount of β-sitosterol, **(D)** X-ray diffraction patterns recorded at 10 °C and 60 °C at small (SAXS) and wide (WAXS) angles as a function of the amount of β-sitosterol in the milk polar lipid vesicles, **(E)** Confocal laser scanning microscopy images of milk polar lipid vesicles in absence or in presence of β-sitosterol as indicated in the figure (red : nile red fluorescent dye).

Figures

Figure 1

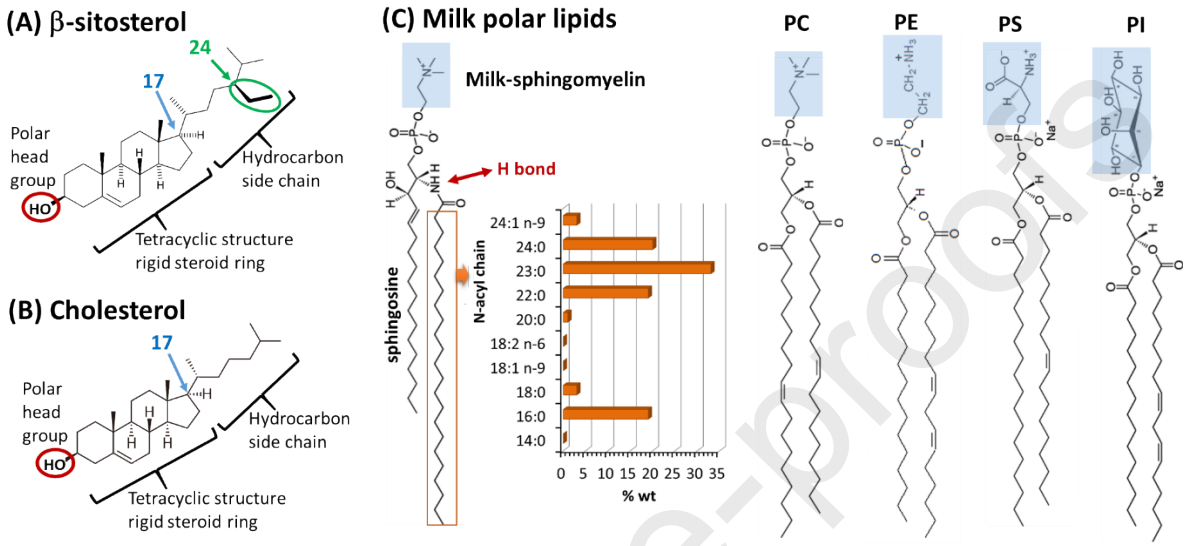

Figure 2

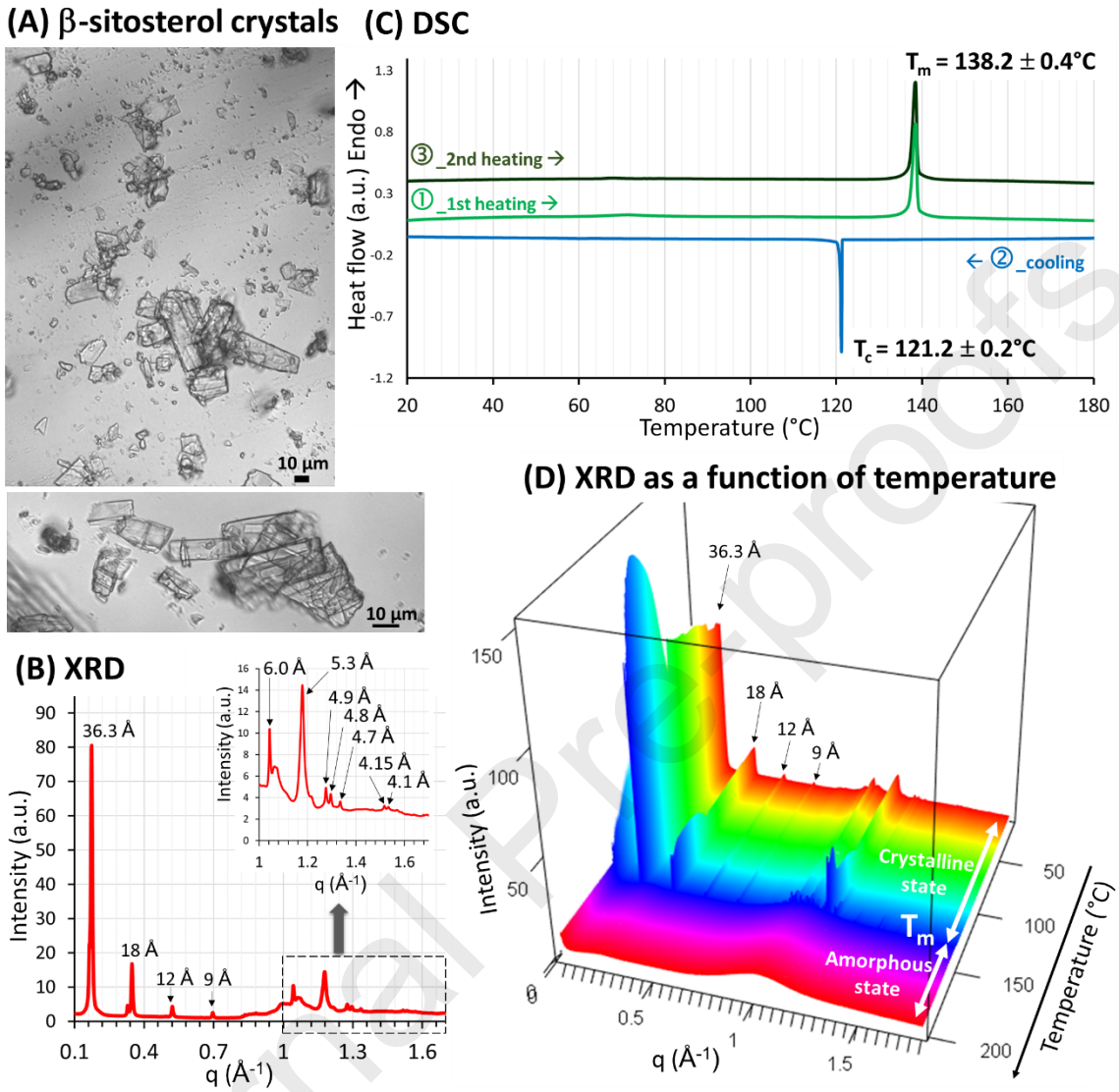

Figure 3

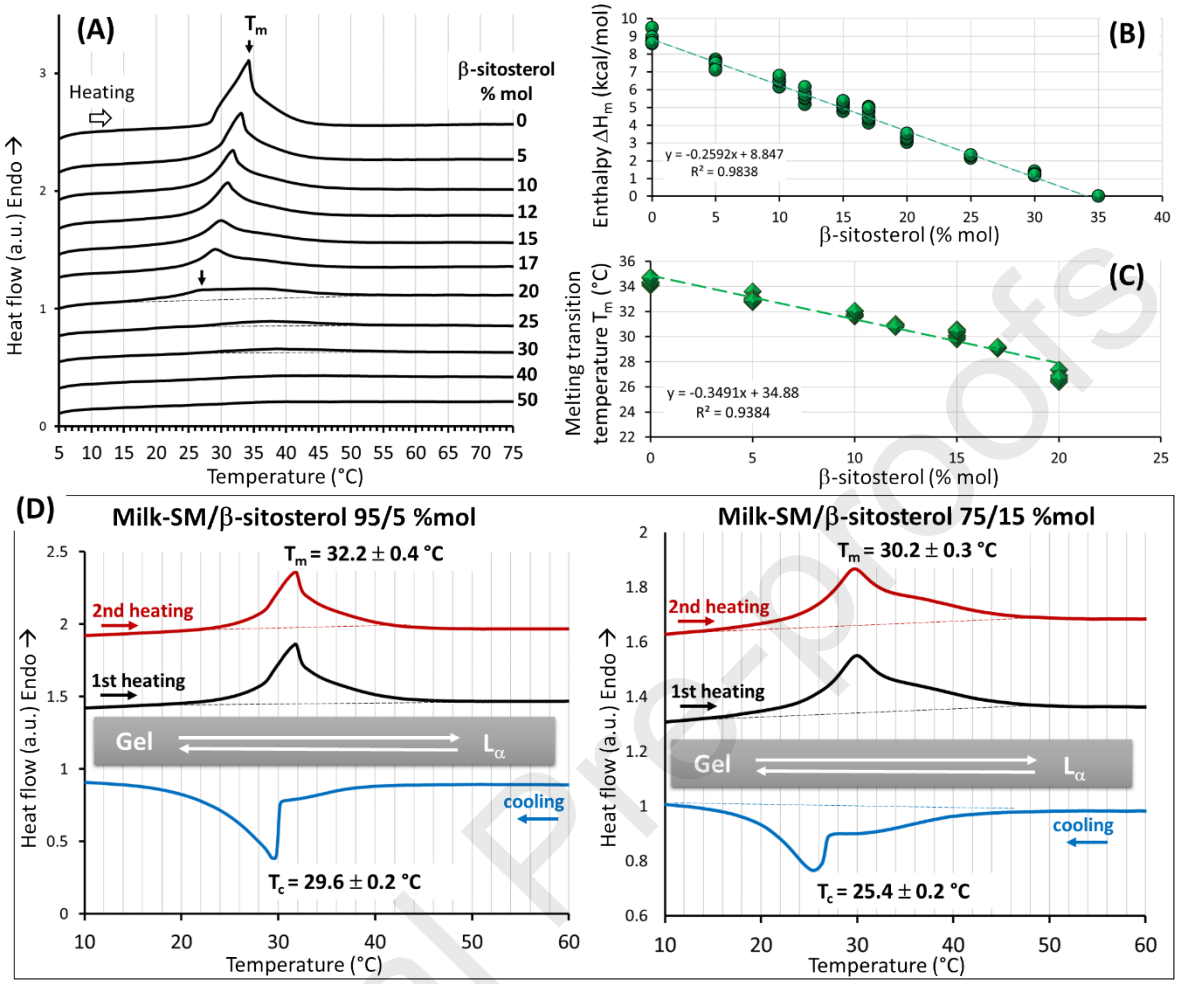

Figure 4

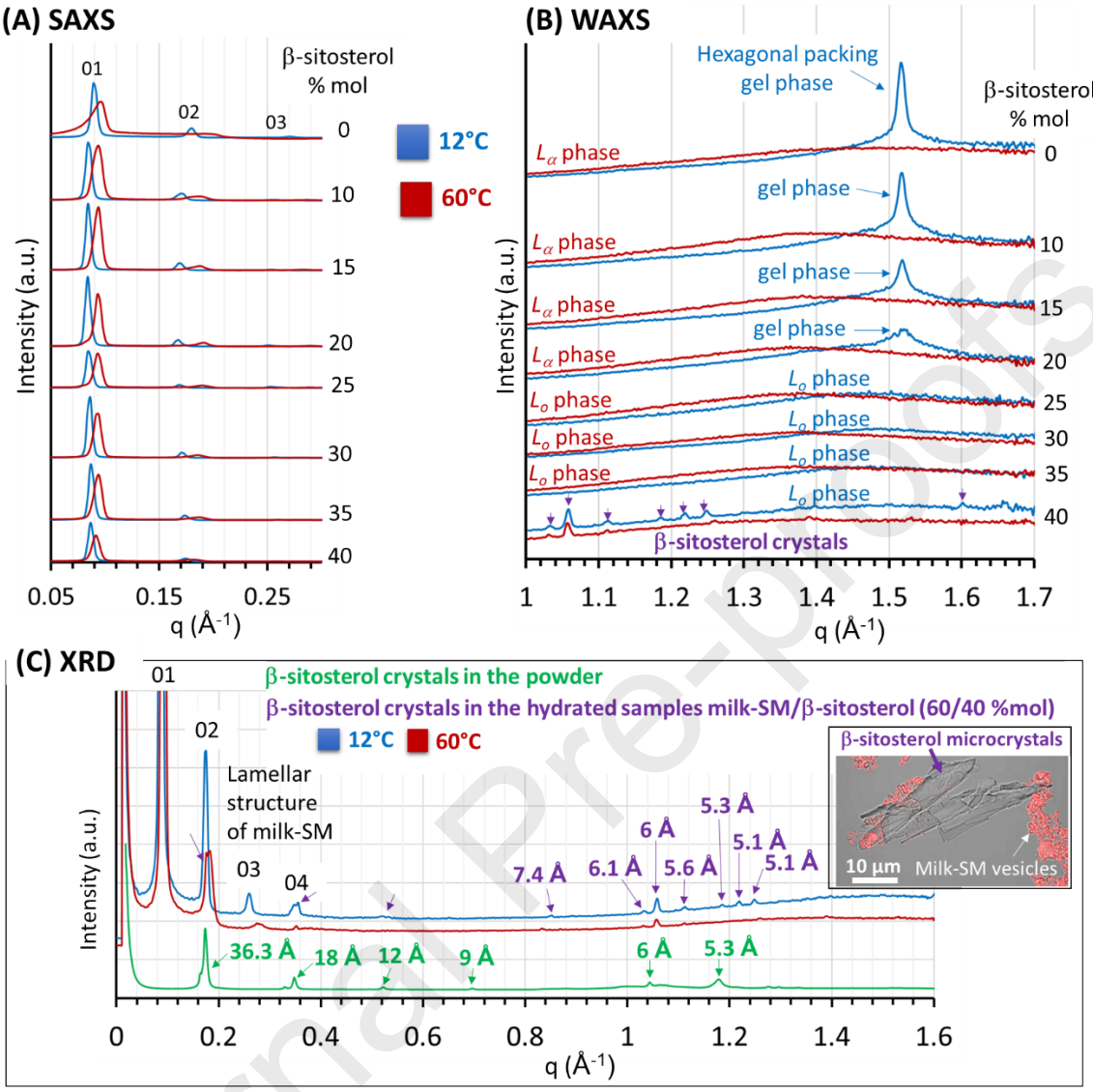

Figure 5

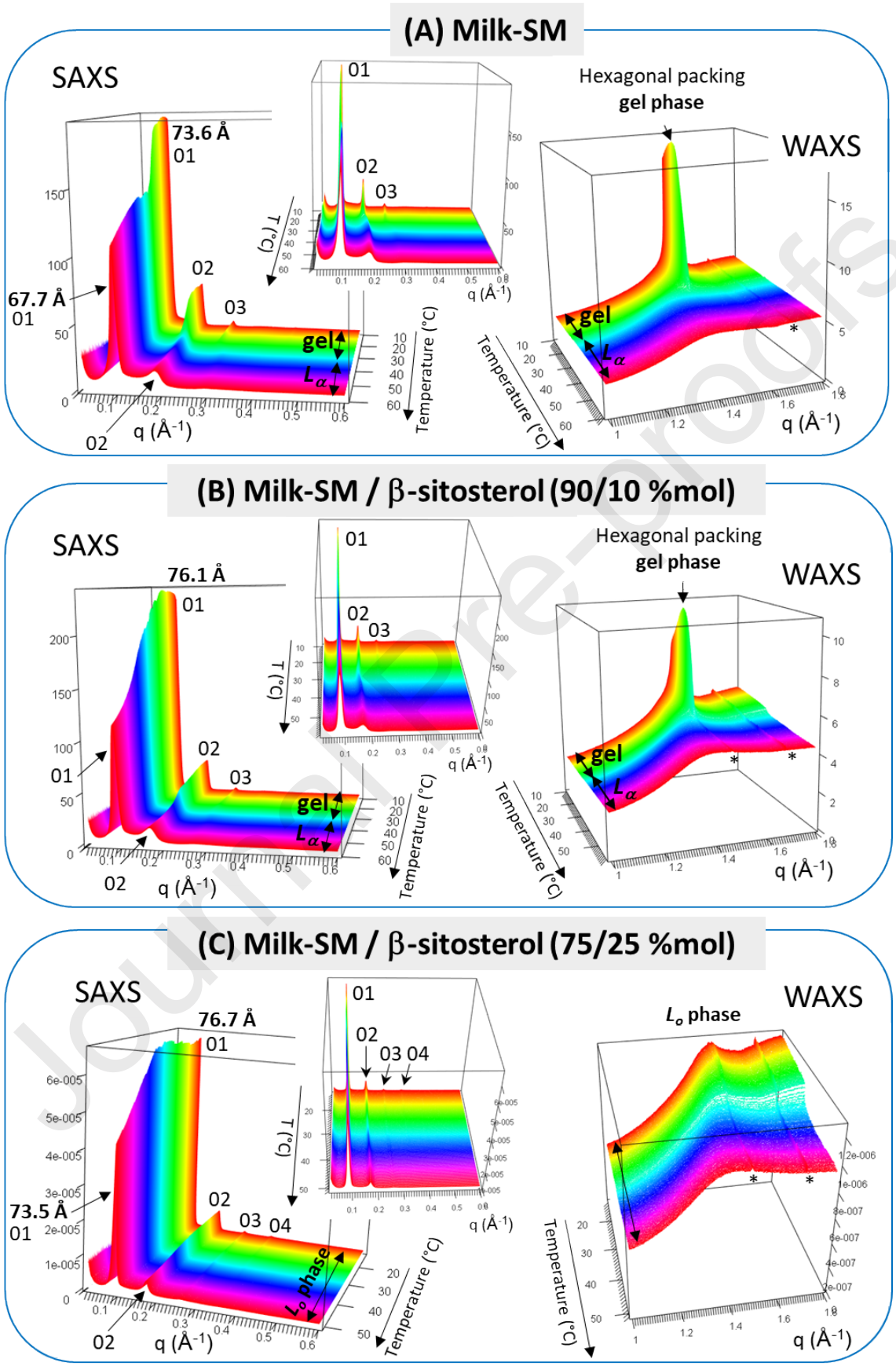
(A) Milk-SM
SAXS
73.6 Å
01
02
03
67.7 Å
gel
L_α
q (Å^{-1})
T (°C)
Temperature (°C)
Hexagonal packing
gel phase
WAXS
(B) Milk-SM / β-sitosterol (90/10 %mol)
SAXS
76.1 Å
01
02
03
gel
L_α
Hexagonal packing
gel phase
WAXS
(C) Milk-SM / β-sitosterol (75/25 %mol)
SAXS
76.7 Å
01
02
03 04
73.5 Å
L_o phase
WAXS
L_o phase

Figure 6

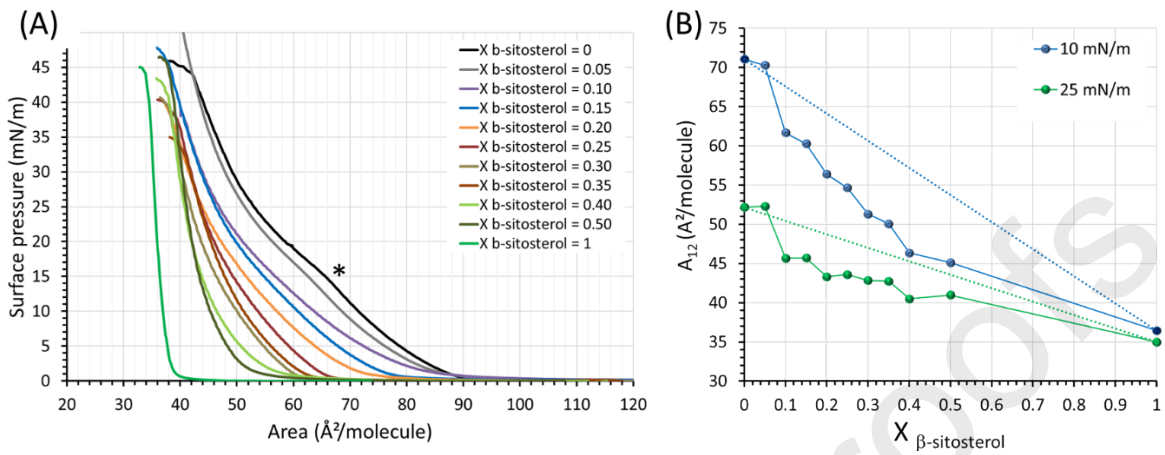

Figure 7

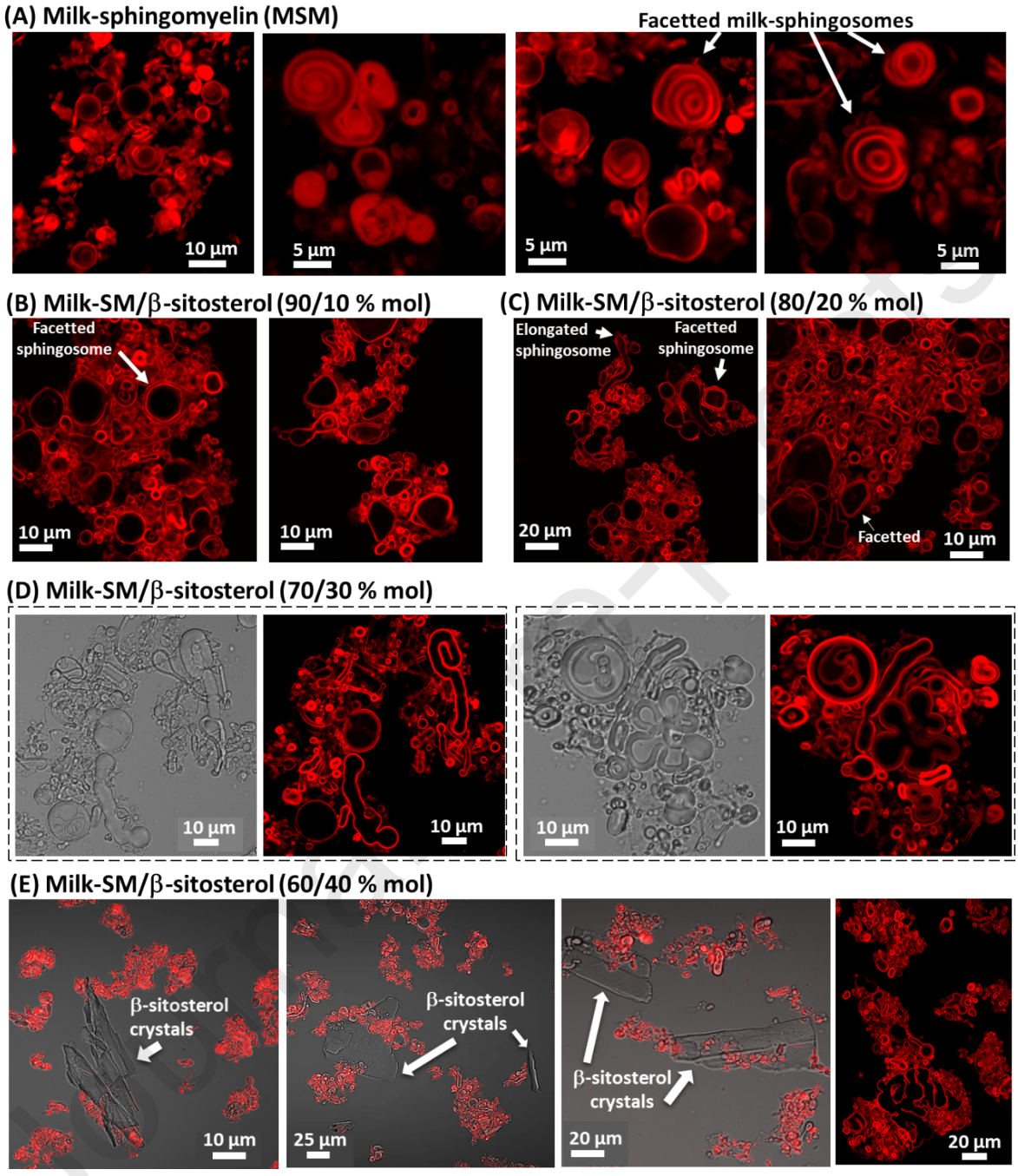
(A) Milk-sphingomyelin (MSM)
Facetted milk-sphingosomes
10 µm
5 µm
5 µm
5 µm
(B) Milk-SM/β-sitosterol (90/10 % mol)
(C) Milk-SM/β-sitosterol (80/20 % mol)
Facetted sphingosome
Elongated sphingosome
Facetted sphingosome
10 µm
10 µm
20 µm
Facetted
10 µm
(D) Milk-SM/β-sitosterol (70/30 % mol)
10 µm
10 µm
10 µm
10 µm
(E) Milk-SM/β-sitosterol (60/40 % mol)
β-sitosterol crystals
β-sitosterol crystals
β-sitosterol crystals
10 µm
25 µm
20 µm
20 µm

Figure 8

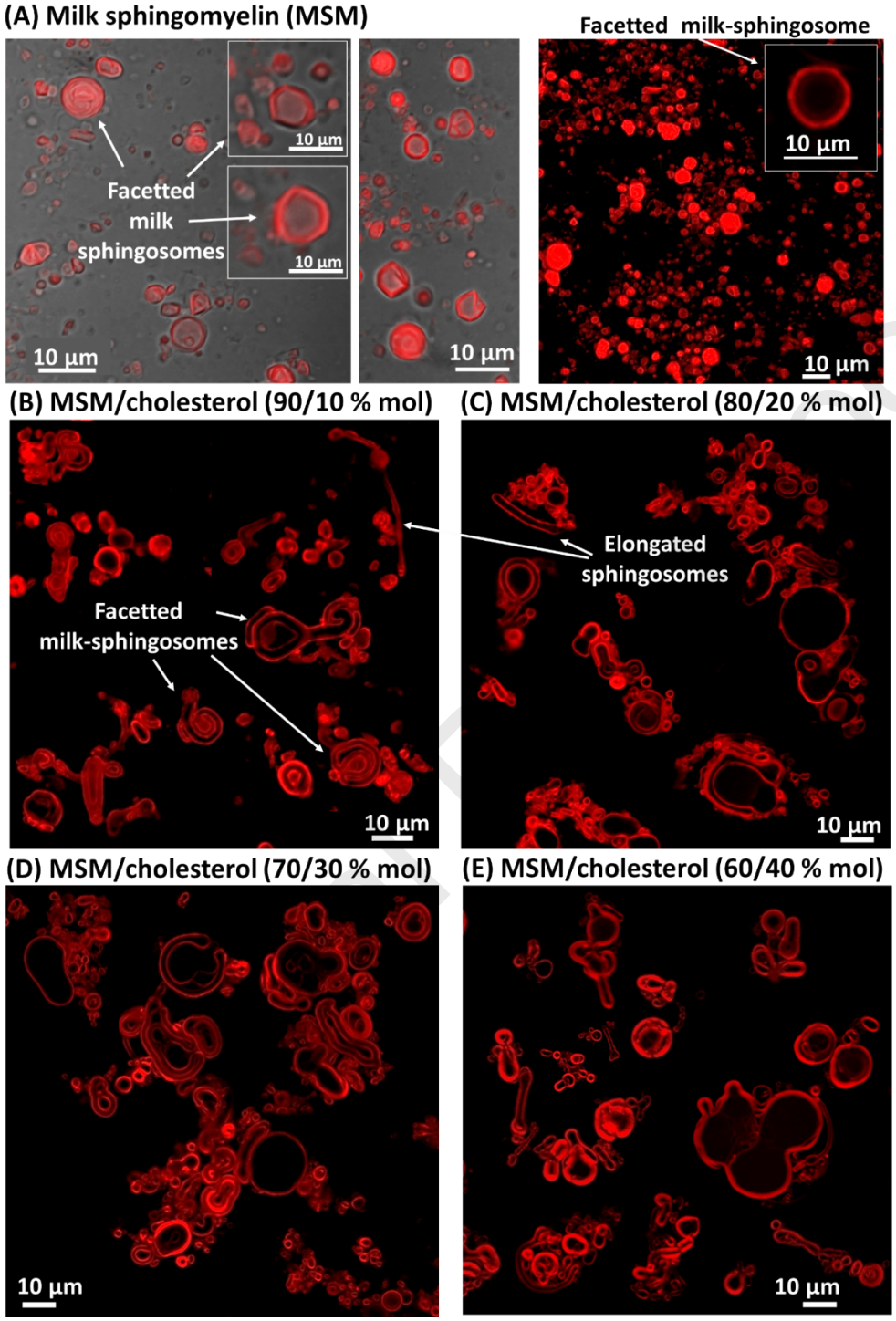

Figure 9

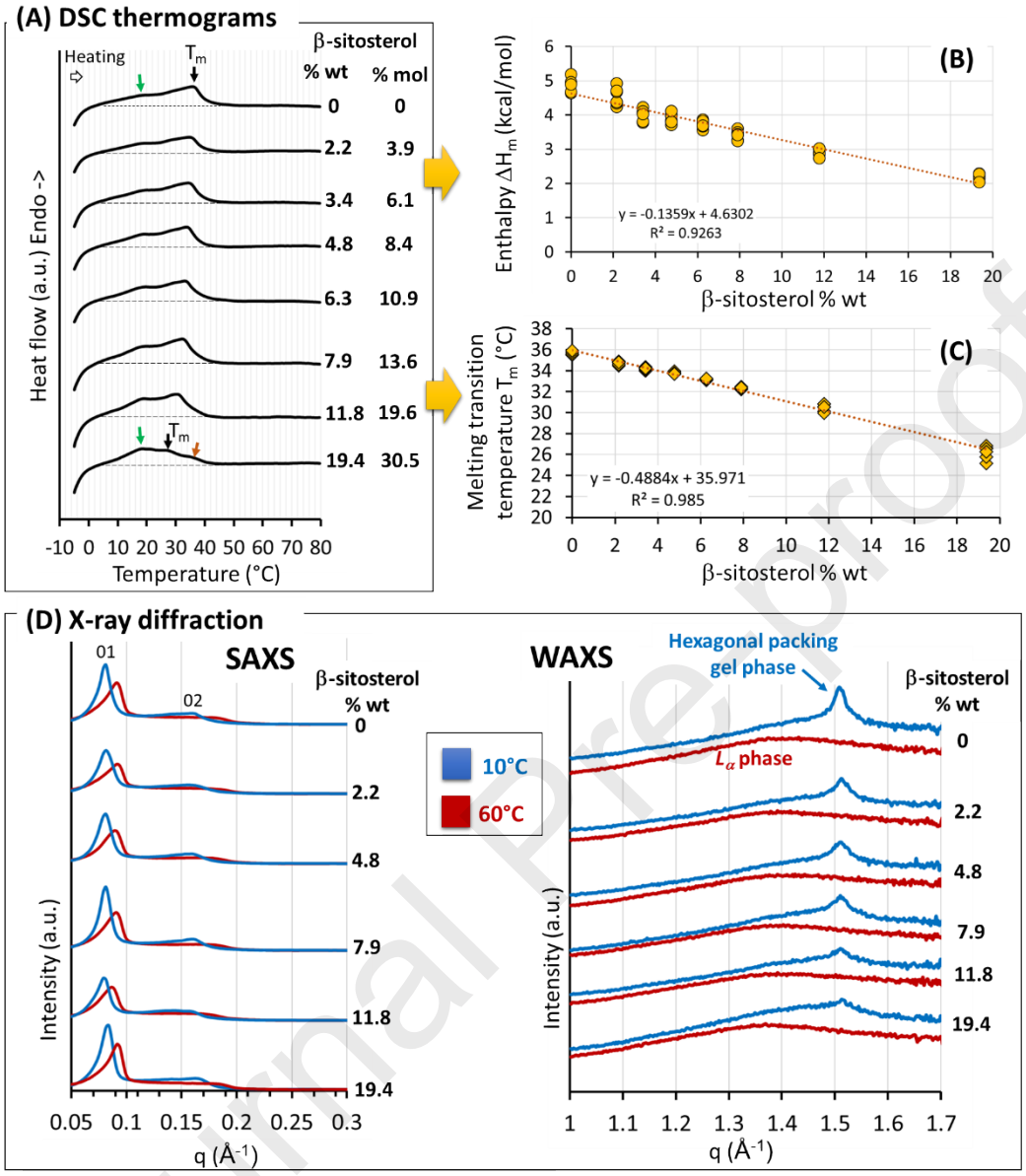
(A) DSC thermograms
β-sitosterol
% wt
% mol
Heating
Tm
0 0
2.2 3.9
3.4 6.1
4.8 8.4
6.3 10.9
7.9 13.6
11.8 19.6
19.4 30.5
Heat flow (a.u.) Endo ->
-10 0 10 20 30 40 50 60 70 80
Temperature (°C)
(B)
Enthalpy ΔHm (kcal/mol)
y = -0.1359x + 4.6302
R² = 0.9263
β-sitosterol % wt
(C)
Melting transition temperature Tm (°C)
y = -0.4884x + 35.971
R² = 0.985
β-sitosterol % wt
(D) X-ray diffraction
SAXS
01
02
β-sitosterol % wt
0
2.2
4.8
7.9
11.8
19.4
10°C
60°C
Intensity (a.u.)
q (Å-1)
WAXS
Hexagonal packing gel phase
Lα phase
β-sitosterol % wt
Intensity (a.u.)
q (Å-1)
(E) Morphology of milk polar lipid vesicles
Milk polar lipids : 0 % wt β-sitosterol
19.4 % wt β-sitosterol
Elongated vesicle
10 µm
10 µm
10 µm

Milk sphingomyelin and polar lipid vesicles as lipid carriers for the solubilisation of plant sterols in foods: softening effect of β-sitosterol on membrane properties inducing changes in sphingosome morphology

Christelle Lopez [a,b,*], Elisabeth David-Briand [a], Virginie Lollier [a,c], Cristelle Mériadec [d], Thomas Bizien [e], Javier Pérez [e], Franck Artzner [d]

[a] INRAE, BIA, F-44316, Nantes, France

[b] INRAE, STLO, F-35000, Rennes, France

[c] INRAE, BIBS Facility, F-44316, Nantes, France

[d] IPR, UMR 6251, CNRS, University of Rennes 1, F-35042, Rennes, France

[e] Synchrotron Soleil, L'Orme des Merisiers, Saint-Aubin BP48, F-91192, Gif-sur-Yvette, France

*Corresponding author : Christelle LOPEZ

christelle.lopez@inrae.fr

The authors declare no conflict of interest

CRediT authorship contribution statement

Christelle Lopez: Conceptualization, Supervision, Writing & editing. **Elisabeth David-Briand**: Investigation. **Cristelle Mériadec**: Investigation. **Virginie Lollier** : Data analysis. **Thomas Bizien**: Investigation. **Javier Pérez** : Supervision. **Franck Artzner**: Conceptualization, Supervision, Writing & editing. All the authors contributed to manuscript writing and approved the final version.

Highlights

- Plant sterols, including β-sitosterol, reduce the risk of cardiovascular disease
- Their low solubility in water and oil limits their formulation and bioaccessibility
- Milk sphingomyelin and polar lipid vesicles are efficient carriers for β-sitosterol in foods
- β-sitosterol is solubilised efficiently into milk sphingomyelin and polar lipid bilayers
- Sphingosomes will contribute in the development of plant sterol enriched functionnal foods

Lopez et al.

Solubilisation of free β-sitosterol in milk sphingomyelin and polar lipid vesicles as carriers: structural characterization of the membranes and sphingosome morphology

GRAPHICAL ABSTRACT